AN ABSTRACT OF THE THESIS OF

Claudio D. Fassardi for the degree of Master of Ocean Engineering in Civil Engineering presented on May 14, 1993.

Title: Analysis of Wave Groups Effects on Rubble Mound Breakwater Stability.

Redacted for Privacy

Abstract approved: _____
Robert Turner Hudspeth

A series of large scale experiments were conducted at the O.H. Hinsdale-Wave Research Laboratory (OHH-WRL) located on the campus of Oregon State University to evaluate the influence of wave groups on the damage of rubble mound breakwaters. The main goal of these experiments was to resolve the controversy regarding the dependency of damage on the characteristics of wave groups.

Realizations approximately 30 minutes long were synthesized from truncated Goda-JONSWAP spectra. Wave groups were characterized by two parameters: 1) the peak enhancement factor, γ, of the Goda-JONSWAP spectrum which correlates with the length of runs; and 2) the envelope exceedance coefficient, α, which correlates with the wave height variability. Realizations were simulated with pairs of the parameters $\{\gamma, \alpha\}$ to test the influence of both short (γ=1) and long (γ=10) length of runs and high ($\alpha > 1$) and low ($\alpha < 1$) wave height variability. The envelope exceedance

coefficient α is computed from the wave height function H(t), or from the envelope A(t), of the sea surface elevation $\eta(t)$.

The experiments were conducted on a rough quarrystone breakwater divided in half longitudinally in order to test simultaneously two armor layers with different armor rock weights. The armor layers were tested with sequences of realizations with increasing significant wave heights.

The experimental results indicated that damage on the armor layers was not influenced by the length of runs (spectral shape). However, it was observed that the wave height variability affects the level of damage on the armor layers.

The envelope exceedance coefficient α was correlated with the groupiness factor $GF = \sigma[H^2(t)]/8m_0$. Random wave trains in wave channels may have exactly the same spectral shape, but produce different levels of damage to the armor layer. The groupiness parameters α or GF may be able to resolve the variability of the mean damage for a given design sea state.

Analysis of Wave Groups Effects on Rubble Mound Breakwater Stability

by

Claudio D. Fassardi

A THESIS

submitted to

Oregon State University

in partial fulfillment of
the requirements for the
degree of

Master of Ocean Engineering

Completed May 14, 1993

Commencement June 1994

APPROVED:

Redacted for Privacy

Professor of Civil Engineering in charge of major

Redacted for Privacy

Head of Department of Civil Engineering

Redacted for Privacy

Dean of Graduate School

Date thesis is presented: May 14, 1993

Typed by Claudio D. Fassardi

ACKNOWLEDGEMENTS

The financial support provided by the following agencies is gratefully acknowledged: Dirección General de Investigación Científica y Técnica, under Grant PB88-0353; the Office of Naval Research under the University Research Initiative (ONR-URI) Contract No. N00014-86-K-0687; and the Oregon Sea Grant and the National Oceanic and Atmospheric Administration, Office of Sea Grant, Dept. of Commerce, under grant NA85AA-D-SG095 (project No. R/CE-21) and appropriations made by the Oregon State Legislature.

TABLE OF CONTENTS

LIST OF FIGURES

LIST OF FIGURES (cont.)

LIST OF TABLES

LIST OF SYMBOLS

$A_{a(e)}$ = accreted (eroded) area,

A_j = amplitude of the j^{th} wave component,

A_z^i = area of active zone of damage of the i^{th} armor rock weight,

$A(x,t)$ = envelope function,

c_1 = parameter, Eq.(30),

C = wave celerity,

$\overline{C}$ = mean wave celerity,

C_g = wave group velocity,

$\overline{C_g}$ = mean group velocity,

$CF^i(k,L)$ = correction function for the i^{th} armor rock weight,

d_n^i = nominal diameter of the i^{th} armor rock weight,

df = frequency interval,

$d\lambda$ = inverse wave length interval,

D' = transformed dimensionless damage level, Eq.(37),

$D^i(k)$ = dimensionless damage level of the i^{th} armor rock weight and realization k,

$\overrightarrow{D}$ = damage vector,

DF = degrees of freedom,

$\overline{E}$ = energy flux,

$\overline{E}(x,t)$ = instantaneous energy flux,

$E[\bullet]$ = expected value of $[\bullet]$,

$EV^i_{M(C)}(k,L)$ = dimensionless measured (corrected) eroded volume function of the i^{th} armor rock weight,

$f_{(p)}$ = (peak) frequency,

LIST OF SYMBOLS (cont.)

f_j = frequency of the j^{th} wave component,

$f_{max(min)}$ = maximum (minimum) cut-off frequency,

$\overline{f}_{(g)}$ = mean (group) frequency,

F_i = F-Test statistic of the i^{th} model,

g = acceleration due to gravity,

GF = groupiness factor,

h = water depth,

h_{ij} = variable, Eq.[40],

H = monochromatic wave height,

H_d^i = design wave height of the i^{th} armor rock weight,

H_* = threshold wave height,

H(x,t) = wave height function,

$H_s(k)$ = significant wave height of the k^{th} realization,

H_{10} = average wave height of the tenth highest waves,

$\overrightarrow{H}$ = wave height ratios matrix,

$i(=\sqrt{-1})$ = imaginary unit number,

J = total number of wave components,

K = number of subrecords,

K_D = stability coefficient,

l_a = horizontal location at which the acreeted area starts,

l_e = horizontal location at which the eroded area ends,

L = longitudinal position at the surveying grid,

m_n = n^{th} spectral moment,

LIST OF SYMBOLS (cont.)

N = total number of data points in the time series,

N_s^i = stability number for i^{th} armor rock weight,

$P_0^i(L)$ = non-damage reference profile function of the i^{th} armor rock weight,

$P_k^i(L)$ = damage profile function corresponding to the k^{th} realization and i^{th} armor rock weight,

RA = number of reverse arrangements,

RSS_i = residual sum of squares of the i^{th} model,

SIWEH(t) = Smoothed Instantaneous Wave Energy History function,

SWL = still water line,

$S_\eta(\bullet)$ = one-sided variance spectral density function of $\eta(x,t)$ in the $(\bullet)$ domain,

$S_{H2}(\bullet)$ = one-sided variance spectral density function of $H^2(x,t)$ in the $(\bullet)$ domain,

t = time,

T_{01} = mean wave period,

$U(\bullet)$ = Heaviside step function of $(\bullet)$,

W_i = mean weight of the i^{th} armor rock,

x = horizontal coordinate,

z(t) = analytic function,

Z = regression analysis group identifier variable,

α = envelope exceedance coefficient,

α' = Eq. (23b),

β = slope angle,

$\Gamma_\eta(\bullet)$ = (unit variance) envelope spectral density in the $(\bullet)$ domain,

LIST OF SYMBOLS (cont.)

γ = peak enhancement factor,

Δ = relative mass density of submerged rock,

$\Delta_c^i(k)$ = EV(k,26) non-closure value for the k^{th} realization,

ΔH_n = variable, Eq.(23c),

Δf = discrete frequency interval,

Δt = sampling time interval,

Δx = horizontal space interval,

$\Delta\lambda$ = inverse wave length interval,

ϵ = regression line parameter,

$\vec{\epsilon}$ = regression line parameter vector,

$\eta(x,t)$ = sea surface elevation,

$\hat{\eta}(x,t)$ = Hilbert Transform of $\eta(x,t)$,

$\eta_\psi(x,t)$ = phase shifted realization,

θ_j = random phase angle of the j^{th} wave component,

$\Theta(t)$ = instantaneous phase function,

κ = permeability,

λ_j = inverse wavelength of the j^{th} wave component,

$\lambda_{max(min)}$ = inverse wave length corresponding to $f_{max(min)}$,

$\overline{\lambda}_{(g)}$ = mean (group) inverse wave length,

μ = parameter, Eq.(30),

ν = level of significance,

$\rho_{w(r)}$ = mass density of the water (rock),

$\sigma[\bullet]$ = standard deviation of [•],

$\sigma^2[\bullet]$ = variance of [•],

LIST OF SYMBOLS (cont.)

χ = parameter, Eq.(46),

ψ = phase angle.

ANALYSIS OF WAVE GROUPS EFFECTS ON RUBBLE MOUND BREAKWATER STABILITY

1. INTRODUCTION

The natural tendency of sea waves to form groups in a random wave field has been recognized as a phenomena of a significant influence in a variety of coastal processes and ocean engineering problems. Medina and Hudspeth (1990) reviewed most of these problems and interrelated in a unified manner the most common methods of wave groups analyses. Although the effects of wave groups on the damage of the armor layer of rubble mound breakwaters have been considered by many authors, a rational method for incorporating wave groups into the design of rubble mound breakwaters has yet to be developed.

Current design methods for armor layers follow the design methodology proposed by the Shore Protection Manual (SPM, 1984) which relates the design of the armor layer to a single representative wave height which corresponds to the design sea state. The SPM methodology does not incorporate the effects of wave groupiness, wave period or duration of the design sea state.

Bruun (1981) reviewed the design of mound breakwaters and emphasized that the damage of these structures is sensitive to wave groups and concluded that wave grouping characteristics should be incorporated into their design.

Evidence of the importance of wave groups has also been reported by Johnson et al. (1978) and Burchart (1979). Van der Meer (1988) proposed 2 new formulae, discriminating between plunging and surging waves, which considered the influence of the duration and wave periods of the design sea state. However, he concluded that wave grouping characteristics and spectral shape have only a minor influence on damage. Recently, Medina and McDougal (1990) reanalyzed the experimental data from Van der Meer (1988), and found that rubble mound breakwaters were more stable against sea states with long wave groups, which appears contrary to intuition.

In order to evaluate the influence of wave groups on the damage of rubble mound breakwaters, a series of large scale experiments were conducted at the O.H. Hinsdale Wave Research Laboratory (OHH-WRL) located on the campus of Oregon State University. The main goal of these experiments was to resolve the controversy regarding the dependency of damage on wave groups characteristics.

2. ENVELOPE AND WAVE HEIGHT FUNCTIONS

Rye (1982) reviewed the different wave groups parameters and methodologies and concluded that wave groups measured from field data compared quite well with those numerically simulated with linear algorithms. The validity of the linear model was also obtained by Goda (1983), Elgar et al. (1984,1985) and Battjes and Vledder (1984) in non-shallow waters.

In his classic treatise on random noise, Rice (1954) developed an extensive theory that may also be applied to linear surface gravity waves (see also Bracewell (1986), Bendat and Piersol (1986), and Dugundji (1958)). The envelope, A(t), of the sea surface elevation, $\eta(t)$, appears to be an appropriate tool for analyzing wave groups. Medina and Hudspeth (1987) and Hudspeth and Medina (1988) used the envelope, A(t), of the sea surface elevation, $\eta(t)$, to analyze some of the most important aspects of wave groups in a random sea state.

Assuming that the sea surface elevation at a given location is a stationary, ergodic and Gaussian process having a one-sided variance spectral density, $S_\eta(f)$, a realization may be approximated by

$$\eta(t) = \sum_{j=1}^{J} A_j \cos(2\pi f_j t + \theta_j) \qquad (1)$$

where J = total number of wave components in the realization, A_j, f_j, and θ_j = the amplitude, the frequency and random phase angle, respectively, of the j^{th} wave component. The random phase angle is uniformly distributed in the interval U[0,2π]. The amplitude of each wave component, A_j, and the one-sided variance spectral density, $S_\eta(f)$, are related by [Tuah and Hudspeth (1982)]

$$A_j^2 = 2S_\eta(f_j)\Delta f \tag{2}$$

where Δf = frequency interval. The n^{th} spectral moment is defined by

$$m_n = \int_0^\infty f^n S_\eta(f)\, df \tag{3}$$

The Hilbert Transform $\hat{\eta}(t)$ of $\eta(t)$ is defined by [Bendat and Piersol (1986)]

$$\hat{\eta}(t) = \sum_{j=1}^{J} A_j \sin(2\pi f_j t + \theta_j) \tag{4a}$$

$$= \sum_{j=1}^{J} A_j \cos(2\pi f_j t + \theta_j - \frac{\pi}{2}) \tag{4b}$$

An analytic function z(t) is a complex-valued function defined by

$$z(t) = \eta(t) + i\hat{\eta}(t) \tag{5}$$

where i = $\sqrt{-1}$. Equation (5) can be rewritten in polar form as

$$z(t) = A(t)\exp(i[\Theta(t)+\phi]) \tag{6}$$

where the envelope function, A(t), is defined by

$$A^2(t) = \eta^2(t) + \hat{\eta}^2(t) \tag{7}$$

and $\Theta(t)+\phi$ = instantaneous phase function is given by

$$\Theta(t) + \phi = ARCTAN\left[\frac{\hat{\eta}(t)}{\eta(t)}\right] \tag{8}$$

The wave height function, H(t), is defined as

$$H(t) = 2A(t) \tag{9}$$

A variety of methods have been introduced for analyzing wave groups from one dimensional (1-D) temporal records. However, random waves in 2-D (x,t) wave channels generate an energy flux that varies both in space and time (x,t). Wave group analyses in 2-D wave channel experiments require a precise description of the evolution in time and space of this variable energy flux which is proportional to the local squared wave height and group velocity. The wave celerity, C, and wave group velocity, C_g, have been formally defined only for monochromatic waves. However, useful approximations of mean wave celerity, $\overline{C}$, and mean group velocity, $\overline{C}_g$, may be obtained for random waves. The sea surface elevation in a 2-D wave channel may be approximated by

$$\eta(x,t) = \sum_{j=1}^{J} A_j \cos[2\pi(f_j t - \lambda_j x) + \theta_j] \quad (10)$$

where x and t = space and time parameters, and λ_j = the inverse of the wave length corresponding to the j^{th} wave component computed from the dispersion relationship

$$f_j^2 = \frac{g}{2\pi}\lambda_j \tanh(2\pi\lambda_j h) \quad (11)$$

where h = water depth and g = acceleration due to gravity.

The Hilbert Transform of $\eta(x,t)$ is defined as

$$\hat{\eta}(x,t) = \sum_{j=1}^{J} A_j \sin[2\pi(f_j t - \lambda_j x) + \theta_j] \quad (12)$$

The envelope, A(x,t), and wave height, H(x,t), functions in a 2-D wave channel are given by

$$H(x,t) = 2A(x,t) = 2(\eta^2(t) + \hat{\eta}^2(t))^{1/2} \quad (13)$$

Families of phase-shifted realizations, $\eta_\psi(x,t)$, associated with a single envelope function, A(x,t), that have the same energy flux may be expressed by

$$\eta_\psi(x,t) = \sum_{j=1}^{J} A_j \cos[2\pi(f_j t - \lambda_j x) + (\theta_j - \psi)] \quad (14a)$$

$$= \eta(x,t)\cos\psi + \hat{\eta}(x,t)\sin\psi \quad (14b)$$

where ψ = constant phase shift given to each wave component. Figure 1 shows families of realizations that have the same envelope function and one-sided variance spectral density functions.

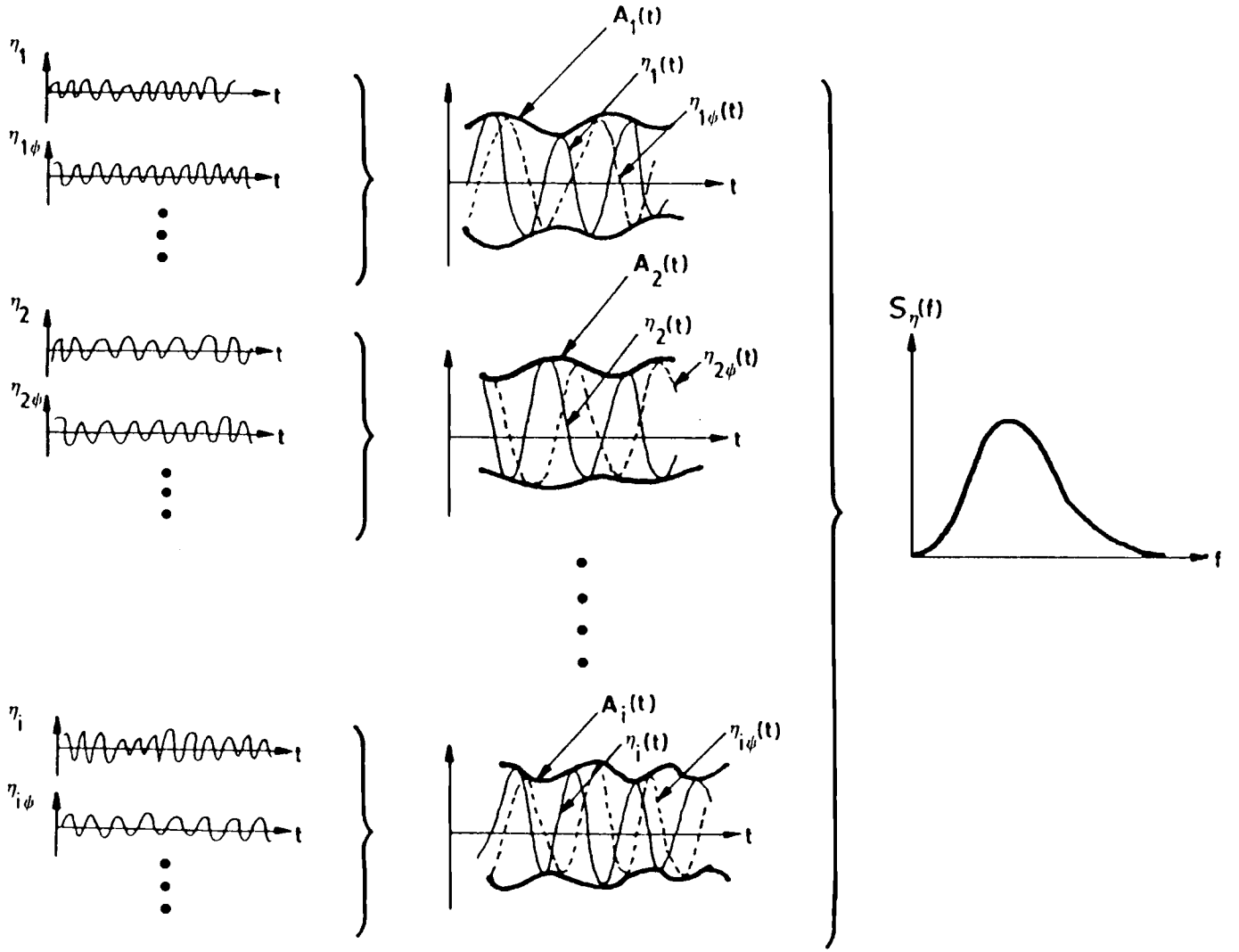

Figure 1. Families of realizations, $\eta_{i\psi}(t)$, with the same envelope function, $A_i(t)$, and spectral density function, $S_\eta(f)$.

The one-sided variance spectral density, $S_\eta(\lambda)$, in the space domain is related to the one-sided variance spectral density, $S_\eta(f)$, in the time domain according to the dispersion relationship, Eq.(11), and

$$S_\eta(\lambda)\, d\lambda = S_\eta(f)\, df \tag{15}$$

The envelope spectral density functions (unit variance) $\Gamma_\eta(f)$ and $\Gamma_\eta(\lambda)$, in time and space, respectively, are given by [Hudspeth and Medina (1988)]

$$\Gamma_\eta(f) = \frac{2}{m_0^2} \int_0^\infty S_\eta(y+f)\, S_\eta(y)\, dy \tag{16a}$$

$$\Gamma_\eta(\lambda) = \frac{2}{m_0^2} \int_0^\infty S_\eta(z+\lambda)\, S_\eta(z)\, dz \tag{16b}$$

Note that $\Gamma_\eta(f)$ and $\Gamma_\eta(\lambda)$ defined by Eqs.(16a,b) are not related as the variance spectra of the sea surface elevation are by Eqs.(15 and 11).

From a spectrum measured in a 2-D wave channel experiment, estimates for the mean wave celerity, $\overline{C}$, and mean group velocity, $\overline{C}_g$, may be computed from

$$\overline{C} \approx \frac{\overline{f}}{\overline{\lambda}} \quad ; \quad \overline{C}_g \approx \frac{\overline{f}_g}{\overline{\lambda}_g} \tag{17a,b}$$

where

$$\bar{f} = \frac{\int_{f_{min}}^{f_{max}} f S_\eta(f)\, df}{\int_{f_{min}}^{f_{max}} S_\eta(f)\, df} \quad ; \quad \bar{\lambda} = \frac{\int_{\lambda_{min}}^{\lambda_{max}} \lambda S_\eta(\lambda)\, d\lambda}{\int_{\lambda_{min}}^{\lambda_{max}} S_\eta(\lambda)\, d\lambda} \qquad (18a,b)$$

$$\bar{f}_g = \frac{\int_{f_{min}}^{f_{max}} f \Gamma_\eta(f)\, df}{\int_{f_{min}}^{f_{max}} \Gamma_\eta(f)\, df} \quad ; \quad \bar{\lambda}_g = \frac{\int_{\lambda_{min}}^{\lambda_{max}} \lambda \Gamma_\eta(\lambda)\, d\lambda}{\int_{\lambda_{min}}^{\lambda_{max}} \Gamma_\eta(\lambda)\, d\lambda} \qquad (19a,b)$$

where $f_{max(min)}$= maximum (minimum) cut-off frequencies, $\lambda_{max(min)}$= maximum (minimum) cut-off inverse wave lengths related to $f_{max(min)}$ by Eq.(11), $\bar{f}$ = mean frequency, $\bar{\lambda}$ = mean inverse wave length, $\bar{f}_g$ = mean group frequency, and $\bar{\lambda}_g$ = mean group inverse wave length. Figure 2 illustrates the (unit variance) one-sided variance spectral density functions $S_\eta(f)$ and $S_\eta(\lambda)$, and (unit variance) envelope spectral density functions $\Gamma_\eta(f)$ and $\Gamma_\eta(\lambda)$ for a Goda-JONSWAP spectrum [Goda (1985)].

For monochromatic waves the energy flux, $\bar{E}$, is defined as

$$\bar{E} = \rho_w g C_g \frac{H^2}{8} \qquad (20)$$

where ρ_w = mass density of water, and H = monochromatic wave height.

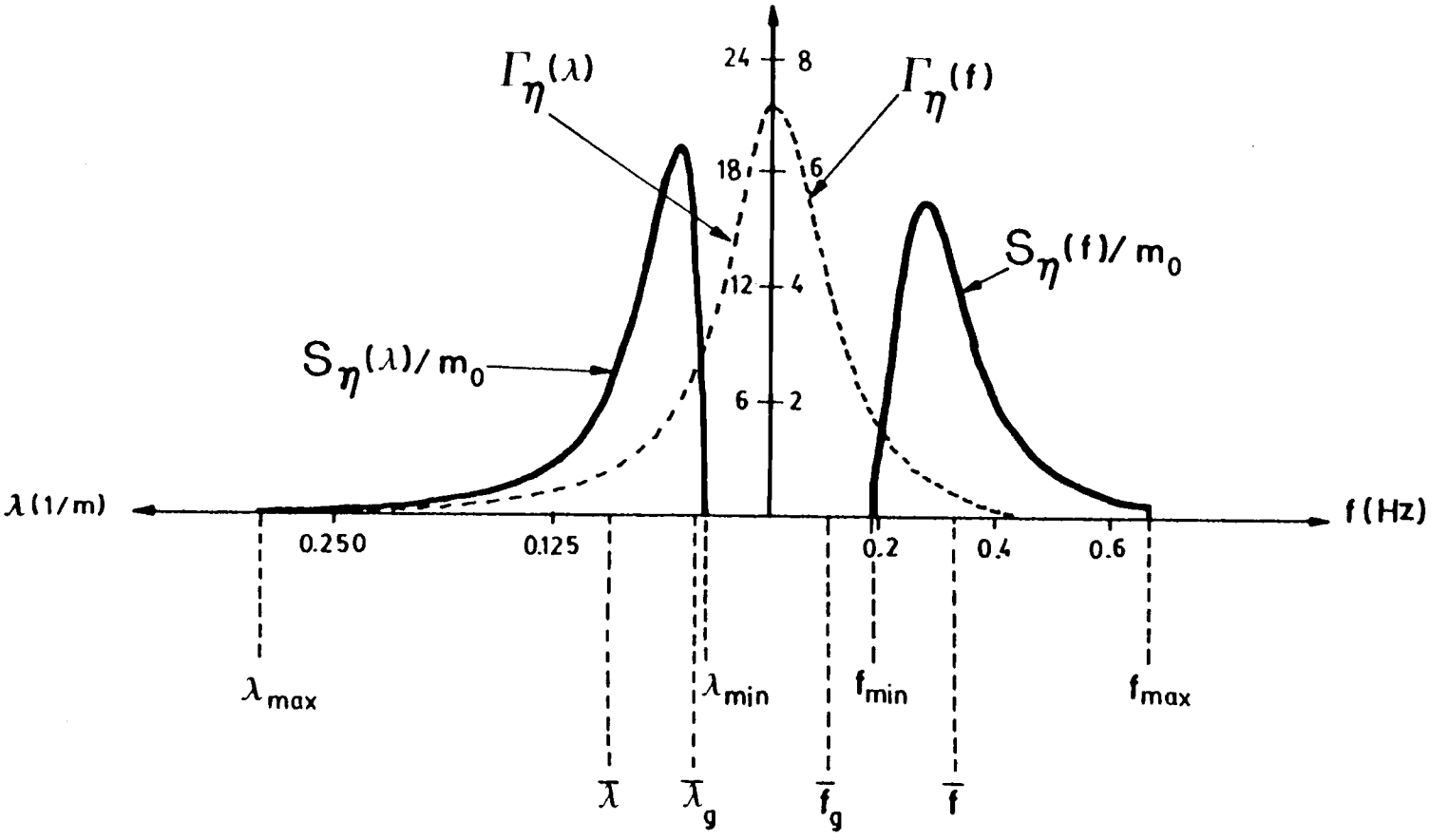

Figure 2. Sea surface elevation spectra (unit variance), $S_\eta(f)$ and $S_\eta(\lambda)$, and envelope spectral densities (unit variance), $\Gamma_\eta(f)$ and $\Gamma_\eta(\lambda)$, in time and space domains respectively.

Equation (20) can be extended for random waves in 2-D to estimate the instantaneous energy flux, $\overline{E}(x,t)$, by

$$\overline{E}(x,t) = \rho_w g \overline{C}_g \frac{H^2(x,t)}{8} \qquad (21)$$

The variance spectra of $H^2(x,t)$, $S_{H2}(f)$ and $S_{H2}(\lambda)$, in time and space domains are given by [Medina and Hudspeth (1987)]

$$S_{H2}(f) \approx 64\ m_0^2\, \Gamma_\eta(f) \quad ; \quad S_{H2}(\lambda) \approx 64\ m_0^2\, \Gamma_\eta(\lambda) \qquad (22a,b)$$

Damage to breakwater armor layers may be influenced by the incident energy flux that is related to $H^2(x,t)$ by Eq.(21). Based on this assumption, it would be reasonable then to use $H(x,t)$ to analyze the influence of wave groups on the damage of breakwater armor layers.

3. ANALYSES OF WAVE GROUPS

The influence of wave groups on the damage of the armor layer of rubble mound breakwaters do not appear to have been treated in a consistent manner in previous studies. The published results of these experiments do not always give a precise indication of the wave grouping characteristics that significantly affected damage. Johnson et al. (1978) indicated that wave trains with long length of runs and high groupiness factor, GF, are more damaging. However, Burchart (1979) suggested that sea states with short length of runs are the most damaging. Finally, Van der Meer (1988) could not identify any significant differences between wave trains with high GF, long length of runs, and narrow spectra and wave trains with low GF, short length of runs, and broad spectra.

The apparent contradiction from these published experimental results may possibly be resolved by the wave grouping characterization model proposed by Mase and Iwagaki (1986). They concluded that at least two parameters are needed to characterize wave groups: 1) one to represent the magnitude of the sequence of high waves or length of runs; and 2) another to represent the magnitude of the variation of the wave heights. Figure 3 shows four different wave height time series classified by Mase and Iwagaki (1986).

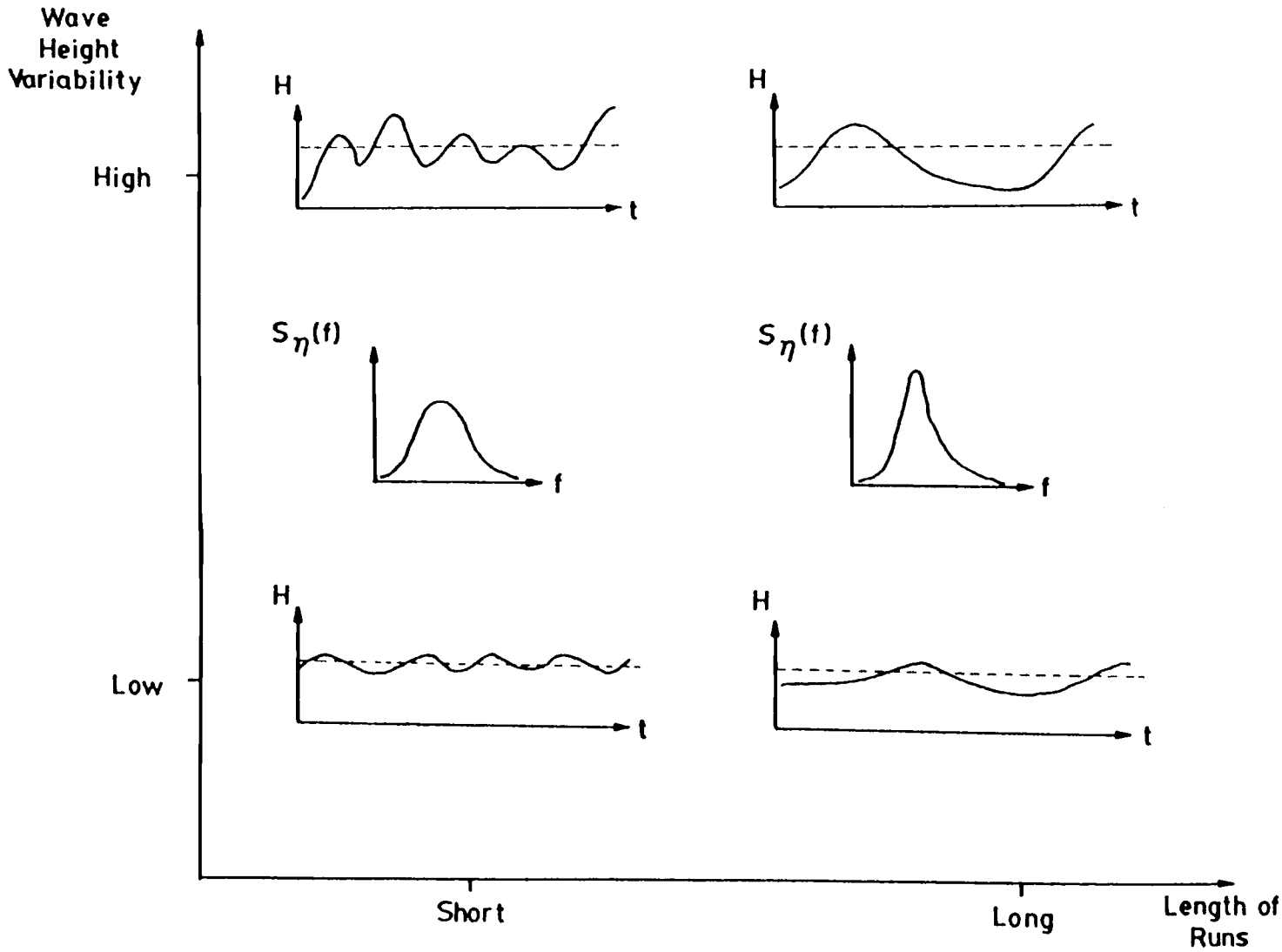

Figure 3. Classification of wave height time series by Mase and Iwagaki (1986)

A run of waves heights is defined as a sequence of waves, the heights of which exceed a predetermined value: e.g., H_s, H_{10}, etc. The length of a run is the number of waves in that run. The length of runs may be characterized by a spectral shape parameter. The relation between spectral shape and length of runs has been shown by Goda (1970). The peak enhancement factor, γ, of the Goda-JONSWAP spectrum [Goda (1985)] was selected to characterize the length of runs. In order to characterize the wave height variability, an empirical envelope exceedance coefficient, α, is proposed. This coefficient is a dimensionless measure of wave height variability of a random sea state above a threshold level, H_*. The average of the tenth highest waves, H_{10}, has been selected as the threshold level H_*. The envelope exceedance coefficient is computed according to

$$\alpha = \frac{\alpha'}{E[\alpha']} \tag{23a}$$

where

$$\alpha' = \frac{1}{N}\sum_{n=1}^{N} (\Delta H_n)^2 \, U(\Delta H_n) \tag{23b}$$

$$\Delta H_n = \frac{H(n\Delta t)}{H_*} - 1 \tag{23c}$$

where E[•] = the expected value of [•], U[•] = Heaviside step function of [•], N = total number of data points in the time

series, Δt = sampling time interval, $H(n\Delta t)$ = discrete wave height function at x=0. The envelope exceedance coefficient, α, may be used as a measure of wave height variability since it depends on $H^2(x,t)$. In addition, since $H^2(x,t)$ is related to $\overline{E}(x,t)$, α also represents a measure of the incident energy flux which may have an influence on the damage of armor layers.

Table 1 and Figure 4 show the wave grouping characteristics proposed by Mase and Iwagaki (1986) and their corresponding parameters.

Wave Groups Characteristics	Parameter
Length of Runs	γ
Wave Height Variability	α

Table 1. Wave groups characteristics and parameters.

The wave group characteristics listed in Table 1 may be correlated with damage to the armor layer by comparing the damage computed from each of the four realizations shown in Fig. 3.

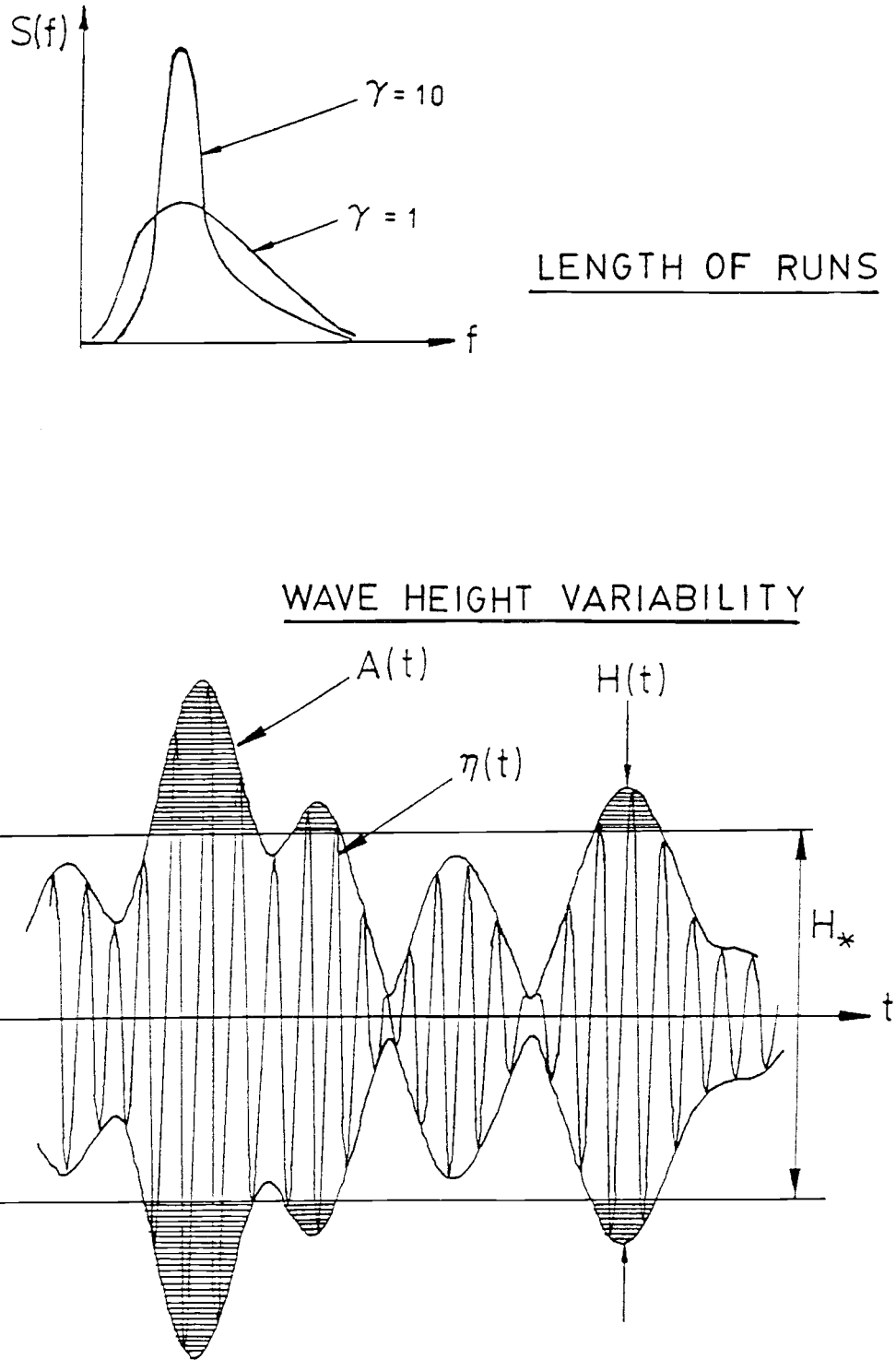

Figure 4. Wave groups characteristics and parameters.

4. TEST FACILITY AND MODEL DESCRIPTION

A schematic of the wave channel at the O.H. Hinsdale-Wave Research Laboratory (OHH-WRL) located at Oregon State University is shown in Figure 5. The wave channel is 104 m long, 3.7 m wide, and 4.6 m deep. The hinged wavemaker moves in either periodic or random motion and is activated by either an electronic function generator or a digital time series synthesized on a digital computer through digital to analog converters (DAC). The digital generation of periodic or random waves uses an inverse Finite Fourier Transform algorithm (FFT) described by Hudspeth and Borgmann (1979). A 112 KW, 24 Mpa oil pump controls the wavemaker through an hydraulic servo-mechanism mounted at 3.05 m above the wavemaker hinge.

The rubble mound breakwater was constructed at the end of the wave channel with a crest high enough to prevent overtopping. The rough quarrystone breakwater model was divided in half longitudinally in order to test simultaneously two different armor layers with mean rock weights W_L=128.5 N and W_S=99.1 N, respectively. The two armor layers were tested with sequences of realizations with consecutive increasing significant wave heights. The significant wave heights, $H_s(k)$ and $H_s(k+1)$, corresponding to realizations k and k+1 respectively, were determined from the armor rock weight ratio according to

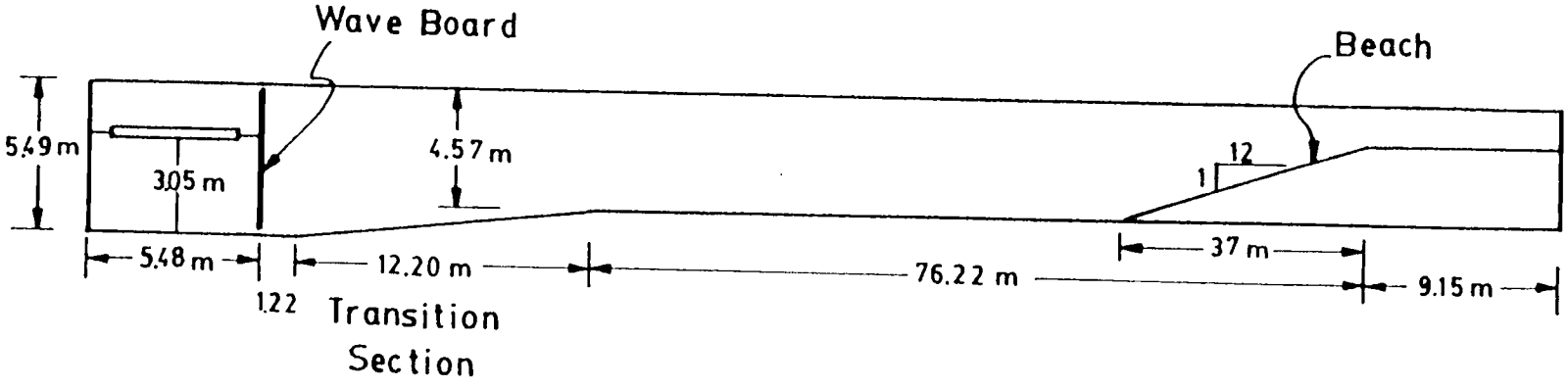

Figure 5. Schematic of OHH-WRL wave channel at OSU.

$$\frac{H_s(k+1)}{H_s(k)} = \left[\frac{W_L}{W_S}\right]^{1/3} \tag{24}$$

According to the SPM (1984) the damage on the armor layer is controlled by the stability number

$$N_s^i(k) = \frac{H_s(k)}{\Delta\, d_n^i} \tag{25a}$$

where

$$\Delta = \left[\left(\frac{\rho_r}{\rho_w}\right) - 1 \right] \tag{25b}$$

$$d_n^i = \left[\frac{W_i}{\rho_r}\right]^{1/3} \tag{25c}$$

and, $N_s^i(k)$ = stability number for the i^{th} armor rock weight from the k^{th} realization, $H_s(k)$ = significant wave height of the k^{th} realization, ρ_r and ρ_w = the mass density of rocks and water respectively, $d_n^i=(W_i/\rho_r)^{1/3}$ is the nominal diameter of the i^{th} armor rock weight, and W_i = mean weight of the i^{th} armor rock. According to Van der Meer (1988), the following factors also influence the damage of the armor layer: slope, permeability of the breakwater, number of waves, and roughness and placement of the armor rocks. In the experiments these secondary factors were held constant.

The stability number for the k^{th} realization and armor rock weight W_S is

$$N_s^S(k) = \frac{H_s(k)}{\Delta \left[\frac{W_S}{\rho_r}\right]^{1/3}} \tag{26}$$

$H_s(k)$ is given by

$$H_s(k) = H_s(k+1) \left[\frac{W_L}{W_S}\right]^{1/3} \tag{27}$$

Substitution of Eq.(27) into Eq.(26) yields to

$$N_s^S(k) = \frac{H_s(k+1) \left[\frac{W_S}{W_L}\right]^{1/3}}{\Delta \left[\frac{W_S}{\rho_r}\right]^{1/3}} = \frac{H_s(k+1)}{\Delta \left[\frac{W_L}{\rho_r}\right]^{1/3}} = N_s^L(k+1) \tag{28}$$

Therefore, since $N_s^S(k) = N_s^L(k+1)$, the damage to the armor layer with rock weight W_L for realization k+1, should be equal to the damage to the armor layer with rock weight W_S for realization k. In this way, it was possible to duplicate the amount of damage data collected during the experiment having the same stability number.

The filter layer rock weight was W_F=21.6 N and the rock specific weight was ρ_r=27.4 kN/m^3. Figure 6 shows a schematic of the breakwater model cross section. Table 2 summarizes the breakwater model characteristics where K_D = stability coefficient [SPM (1984)], β = slope angle, and H_d^i = design wave height for the ith armor rock weight computed according to the Hudson formula [SPM (1984)].

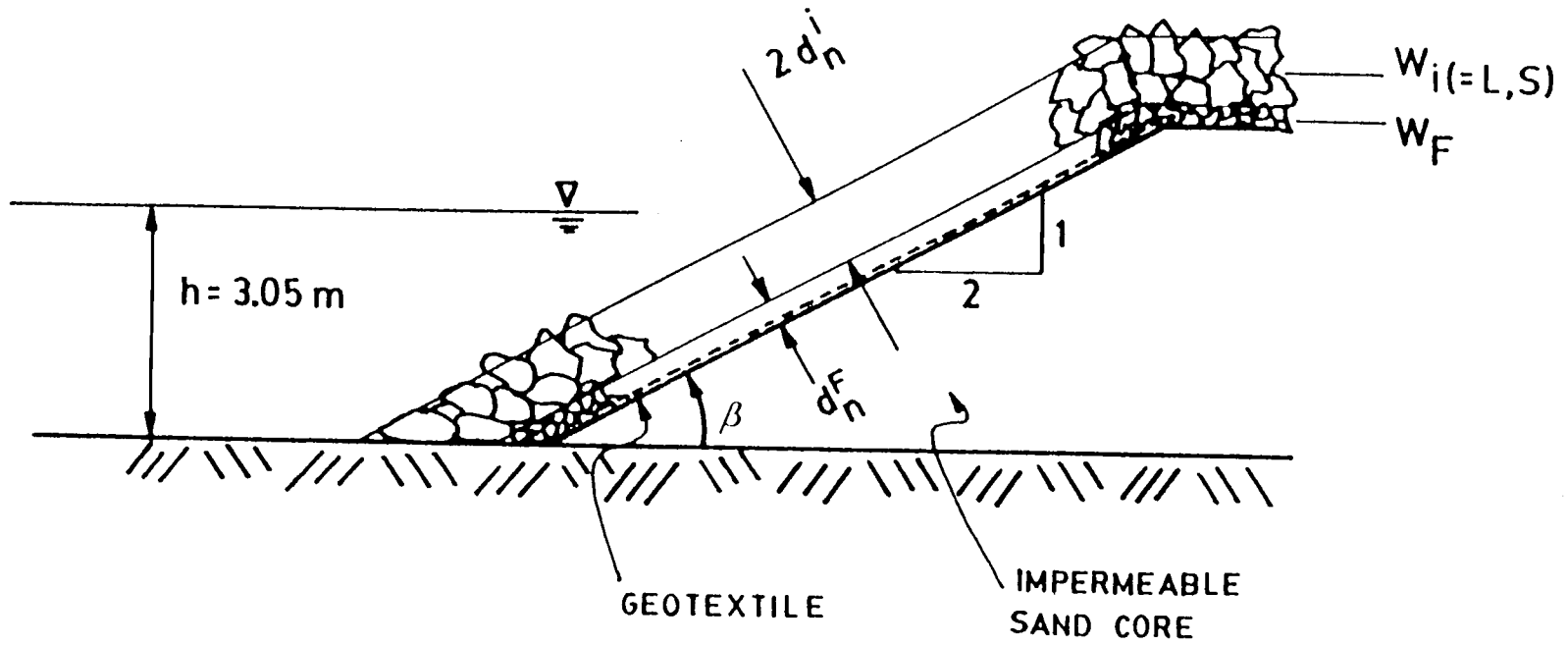

Figure 6. Schematic of the breakwater model cross section.

K_D	cotgβ	W_L [N]	W_S [N]	W_F [N]	ρ_r[kN/m^3]	H_d^L[m]	H_d^S[m]
4	2	128.5	99.1	21.6	27.4	0.599	0.544

Table 2. Summary of breakwater model characteristics.

Figure 7 shows the weight distribution for each armor layer.

Figure 8 shows the location of the instrumentation used. Cross section profiles of each side, sea surface elevations, hydrodynamic pressures, video records of run-up, and visual observations of rock movements were recorded during the experiments. The wave records obtained from the three ultrasonic wave gauges located 10 m in front of the structure were used to resolve the incident wave trains on the structure. The incident and reflected wave trains were resolved using the extension of Kimura (1985) to the method of Goda and Suzuki (1976).

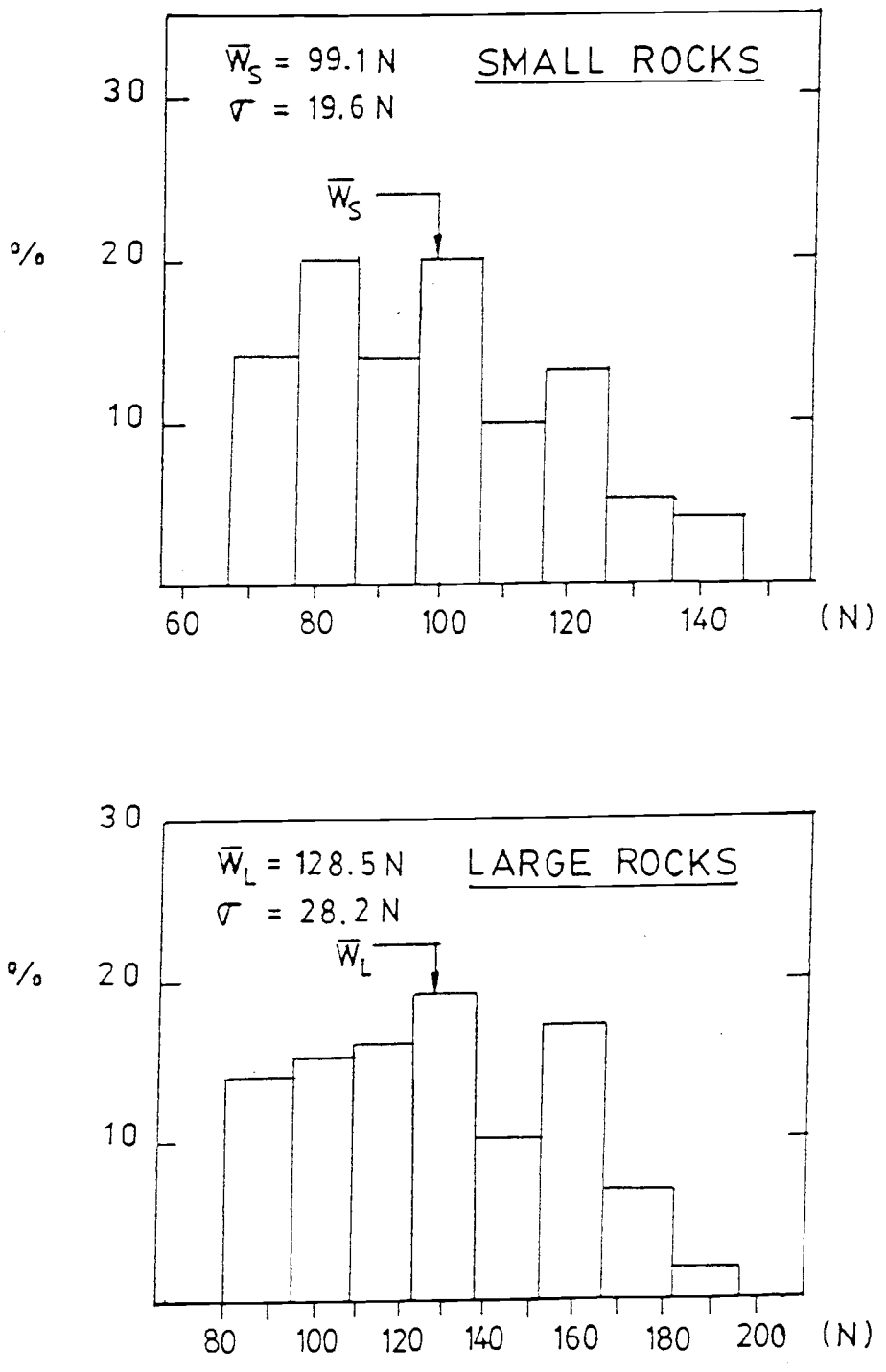

Figure 7. Weight distribution of the armor layers.

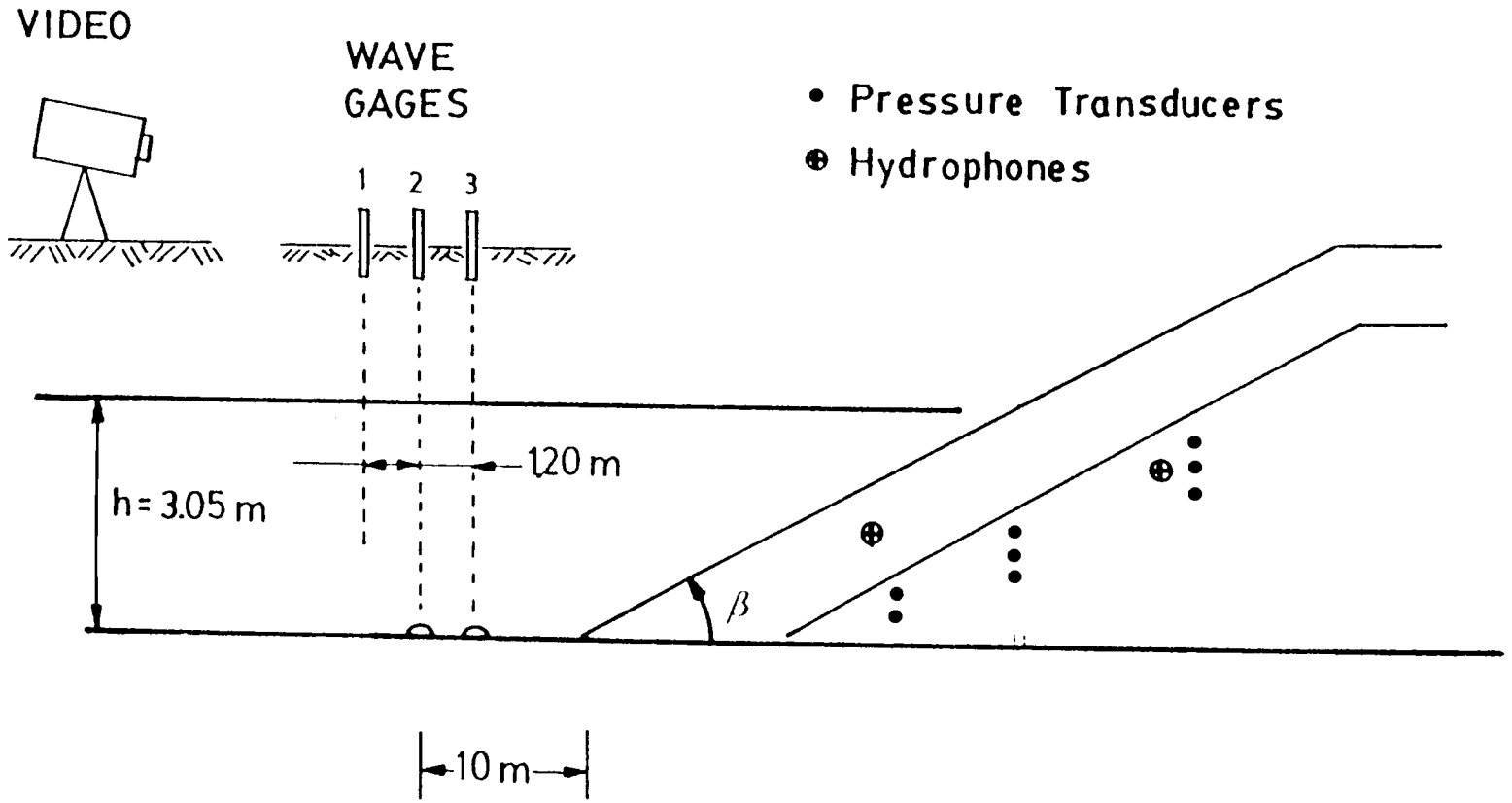

Figure 8. Location of the instrumentation deployed for the experiment.

5. DESCRIPTION OF THE EXPERIMENTS

Two fundamental wave grouping characteristics were considered: 1) the length of runs, characterized by the spectral shape; and 2) the wave height variability characterized by the envelope exceedance coefficient, α. DSA simulated random waves [Tuah and Hudspeth (1982)] were synthesized from Goda-JONSWAP spectra [Goda (1985)]. The peak enhancement factor γ in Goda-JONSWAP spectrum was used to characterize broad (γ=1) and narrow (γ=10) spectra. The mean period, given by

$$T_{01} = \frac{m_0}{m_1} \tag{29}$$

was a constant T_{01}=3 sec for all realizations. The influence of the wave height variability was analyzed by the envelope exceedance coefficient, α. Two different phase spectra were selected for each spectral shape (γ=1 and γ=10) to simulate realizations with relatively high and low α's. The low and high values of α and their corresponding phase spectra were selected from one hundred DSA random wave simulations from two truncated Goda-JONSWAP spectra (γ=1 and γ=10).

The incident wave time series were resolved from the measured partially standing wave records using the method of Kimura (1985). This method is able to resolve incident and reflected wave time series only in a finite frequency

bandwidth. Accordingly, the DSA simulations were synthesized from truncated Goda-JONSWAP spectra [Goda (1985)] defined by

$$S_\eta(f) = c_1 H_s^2 \frac{f_p^4}{f^5} \exp\left[-1.25\left(\frac{f}{f_p}\right)^{-4}\right] \gamma^{\exp\left[-\left(\frac{f}{f_p}-1\right)^2/2\mu^2\right]} \qquad (30)$$

for $f_{min} \le f \le f_{max}$, where f_p = peak frequency, H_s = significant wave height, and c_1 is a dimensionless coefficient that maintains the energy from the untruncated spectrum. Table 3 shows the values of the parameters used in Eq.(30).

γ	c_1	f_p [Hz]	$\frac{f_{min}}{f_p}$	$\frac{f_{max}}{f_p}$	μ $(f \le f_p)$	μ $(f \ge f_p)$
1	1.03746	0.27048	0.7	2.5	0.07	0.09
10	1.01332	0.30578	0.7	2.5	0.07	0.09

Table 3. Parameters used in the truncated Goda-JONSWAP spectrum

The peak frequency, f_p, was selected so that the mean period computed from Eq.(29) was a constant T_{01}=3 sec for each of the realizations.

Sequences of 7 realizations were simulated with the 4 pairs of parameters $\{\gamma, \alpha\}$, shown in Fig. 7, and wave heights in meters determined from

$$H_s(k) = 0.43\left[\frac{W_L}{W_S}\right]^{\frac{k-1}{3}} \quad ; \quad k=1,2,..,7 \qquad (31)$$

where $H_s(k)$ = significant wave height in meters corresponding to the k^{th} realization. Each realization was approximately 30

minutes long and contained N = 2^{15} = 32768 values, at Δt = 0.06 sec. Figure 9 shows the target values of the wave grouping parameters and the notation used to identify the sea states with those parameters: 1) E1: long length of runs (high γ) and high wave height variability ($\alpha>1$); 2) E2: short length of runs (low γ) and high wave height variability ($\alpha>1$); 3) E3: long length of runs (high γ) and low wave height variability ($\alpha<1$); 4) E4: short length of runs and low wave height variability ($\alpha<1$).

Each of the seven realizations in a sequence was shifted by a constant phase $\psi=0, 2\pi/3, 4\pi/3$, and 2π, according to Eq.(14b) to determine the influence on damage from different realizations with the same wave grouping characteristics. Figure 10 shows different realizations having the same envelope function, A(t), shifted by a constant phase ψ.

At the time the experiment was conducted the OHH-WRL did not have direct digital control on the wavemaker that would allow cancellation of waves reflected by the breakwater. The re-reflected waves added energy to the incident wave spectra. In order to evaluate the stationarity of the wave generation process under these conditions, reverse arrangements tests [Bendat and Piersol (1986)] were performed. The results of these tests are presented in Appendix A. These tests demonstrated that the incident wave time series were stationary.

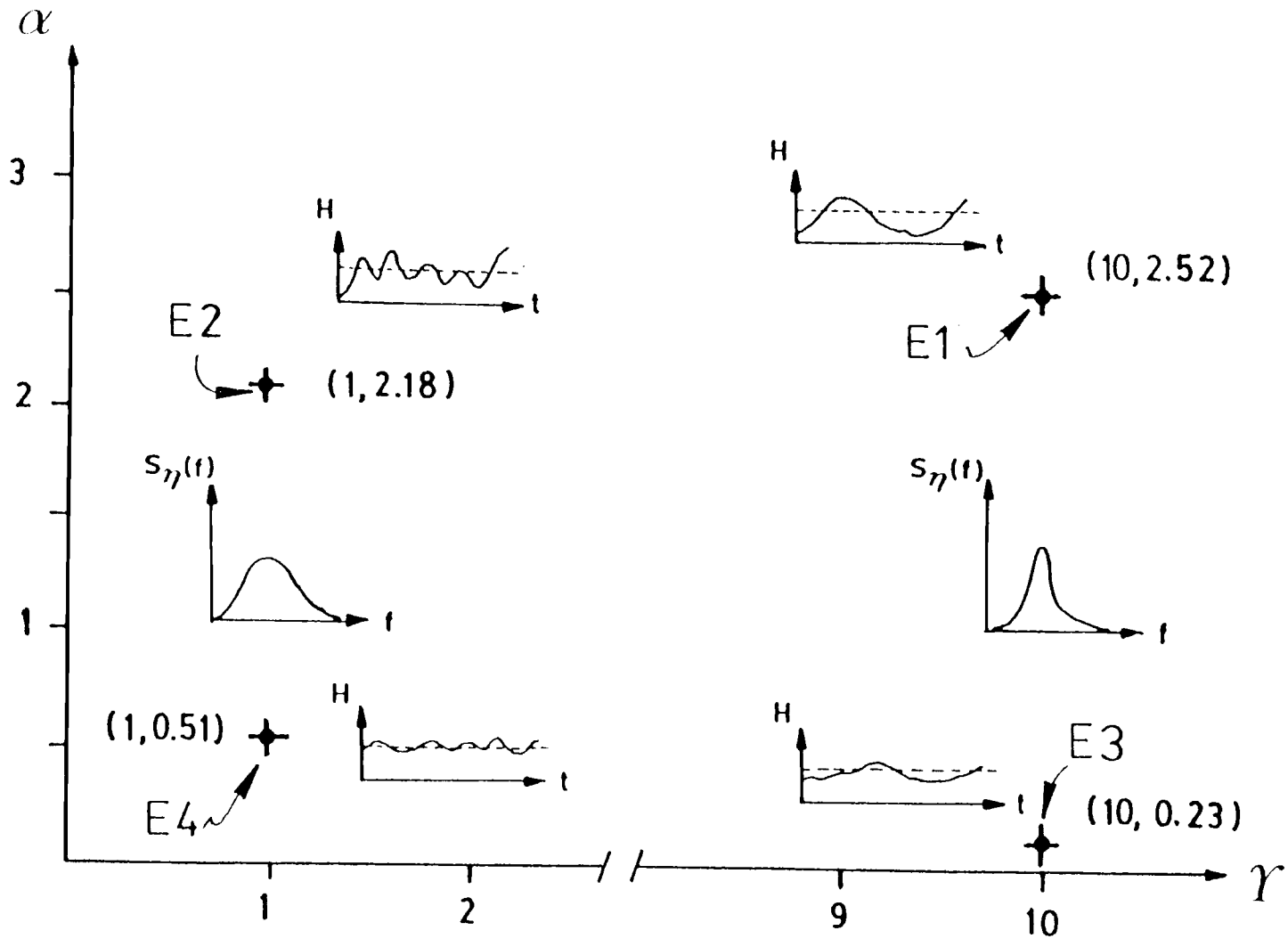

Figure 9. Target values of the wave grouping parameters selected for the experiment.

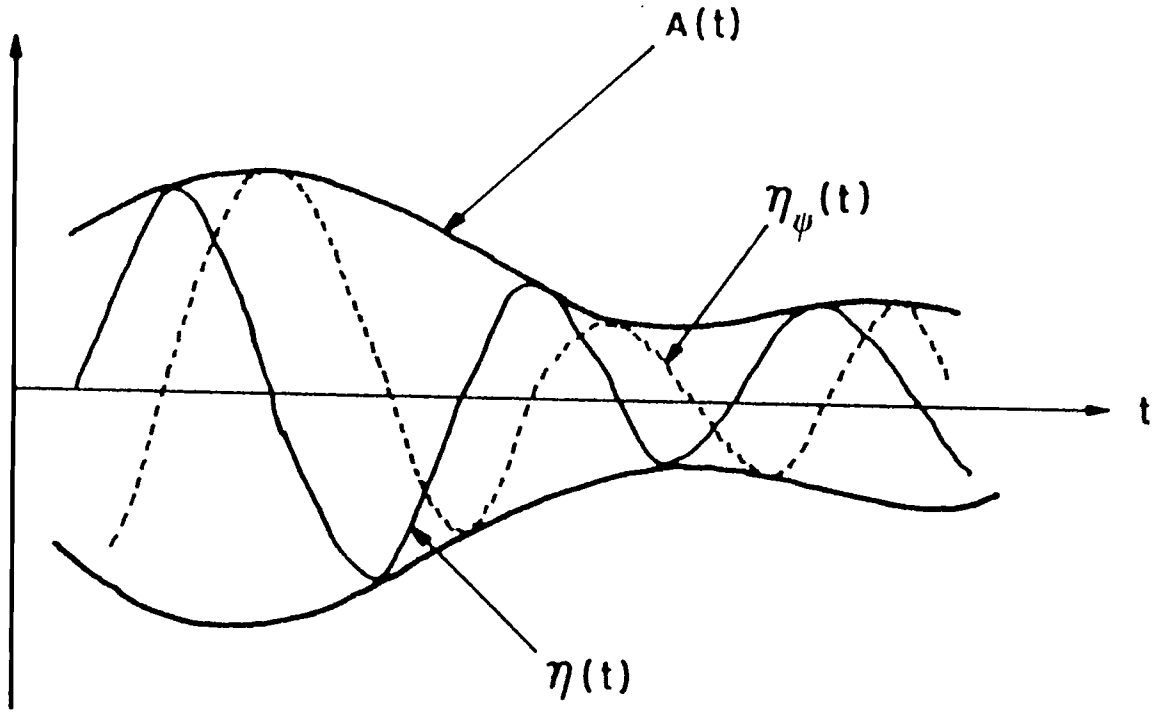

Figure 10. Realizations shifted by a constant phase ψ with the same envelope function, A(t).

6. MEASURED DAMAGE

Cross section profiles on each side of the breakwater were obtained after each run by measuring from the toe to the crest the vertical distance below a reference level to the armor layer in a 52x2 point grid using typical surveying instruments. These vertical measurements were later referenced to the bottom of the wave tank. Figure 11 shows the survey grid.

The surveying procedure for each of the 16 sequences (4 pairs $\{\gamma, \alpha\}$ x 4 constant phase shifts) of the 7 realizations consisted of surveying each side of the breakwater as follows: 1) prior to the first realization to obtain non-damage reference profiles; and 2) after each realization to obtain damage profiles. Each side of the breakwater was rebuilt after the seventh realization.

For each side of the breakwater the profiles measured were used to compute average non-damage reference profiles, $P_0^i(L)$, and damage profiles, $P_k^i(L)$, from realization k at stations L=1,2,..,26 for the i^{th} armor rock weight. Figure 12 illustrates typical non-damage reference and damage profiles for the armor layer with armor rock weight W_S=99.1 N. The accreted area starts at location l_a and the eroded area ends at location l_e.

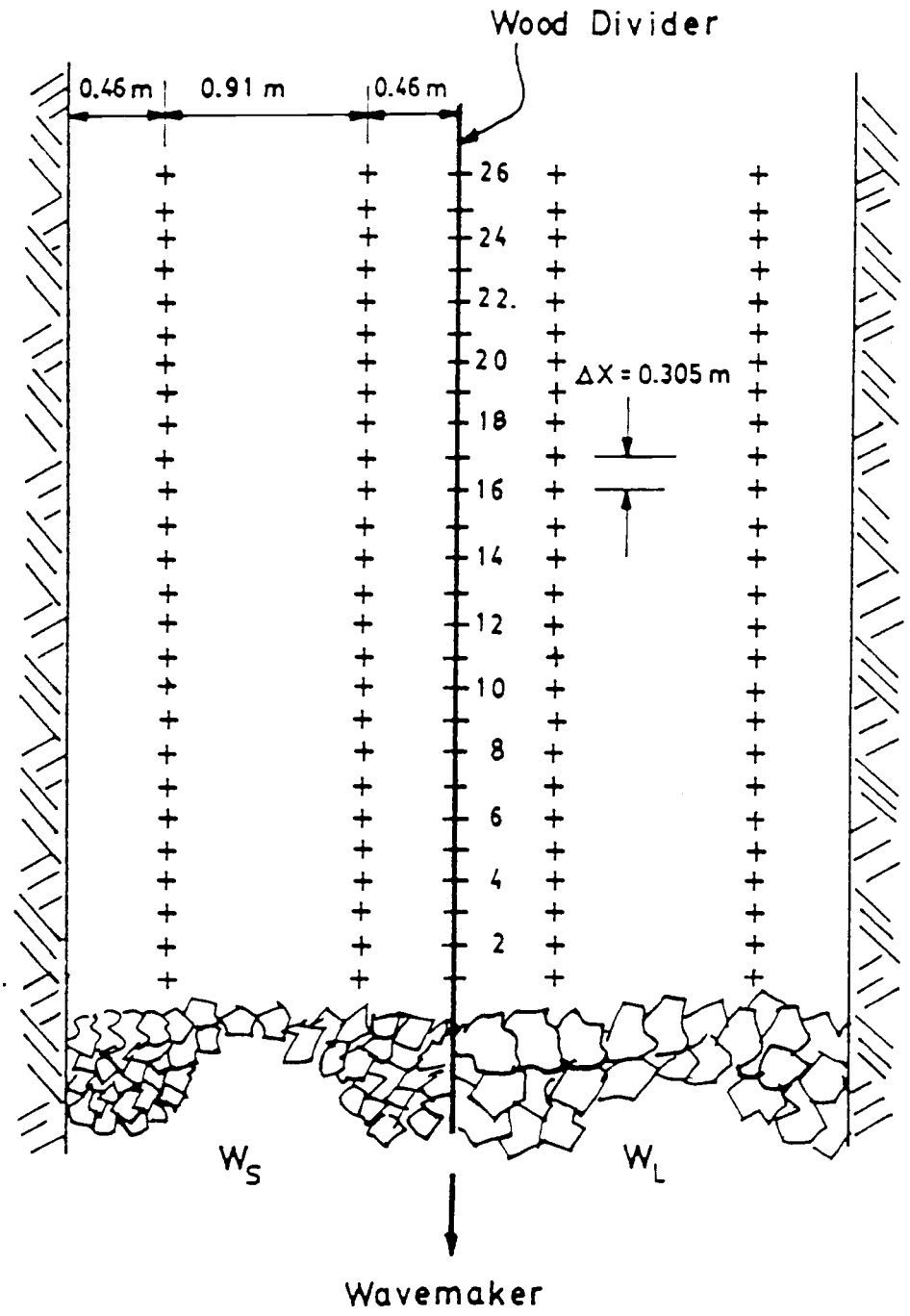

Figure 11. Survey grid and armor layers with rock weights W_L=128.5 N and W_S=99.1 N.

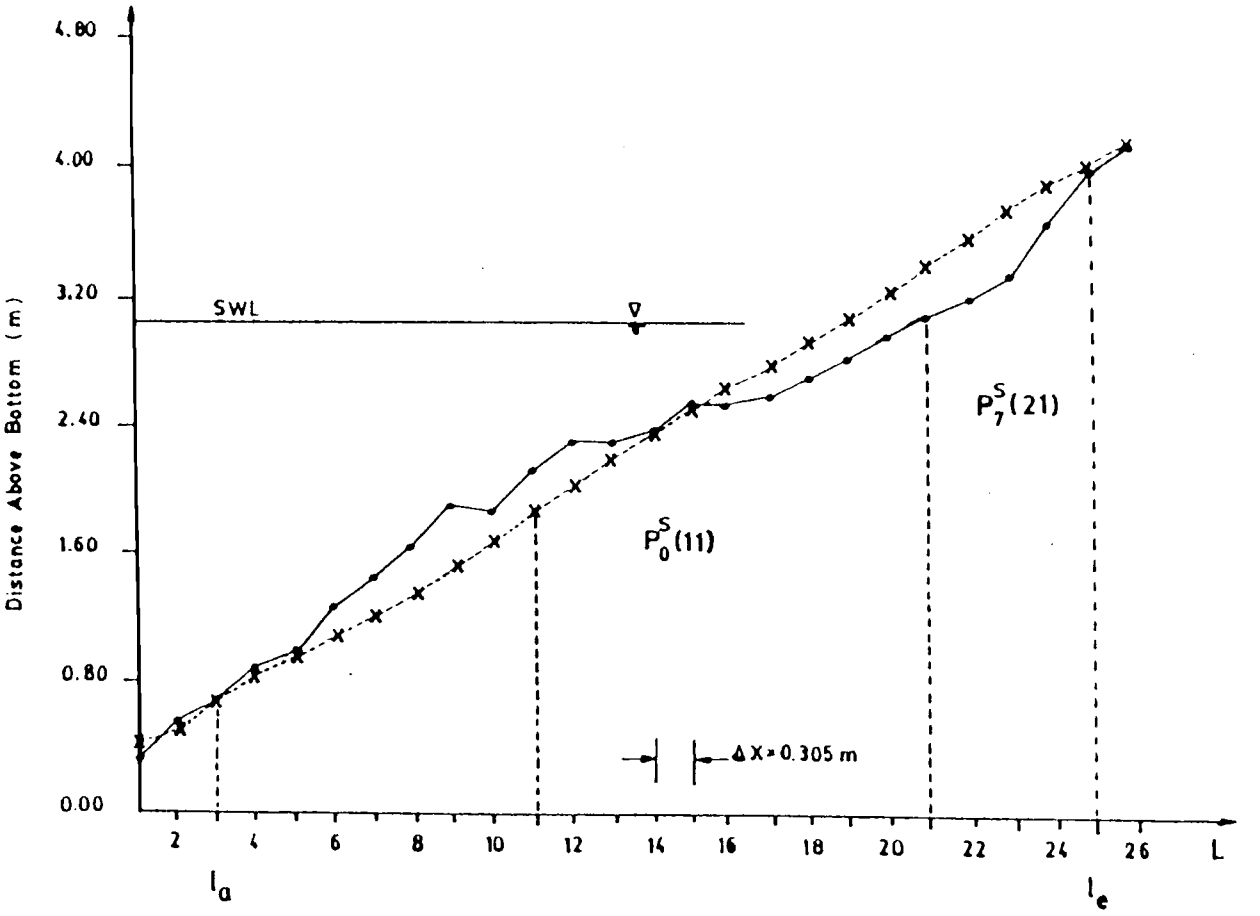

Figure 12. Reference, $P_0^S(L)$, and damage, $P_7^S(L)$, profiles corresponding to a realization with parameters γ=10, α=1.027, ψ=0, and H_s=0.73 m.

For each damage profile, dimensionless measured eroded volume functions $EV_M^i(k,L)$, for run k at station L, were computed by

$$EV_M^i(k,L) = EV_M^i(k,L-1) + \sum_{I=L-1}^{L} \left[P_k^i(1) - P_0^i(1)\right] \frac{\Delta x}{2(d_n^i)^2} \quad ; \quad L=2,..,26 \qquad (32)$$

where $EV_M^i(k,1)=0$; and $\Delta x=0.305$ m horizontal space interval. The k^{th} eroded volume function is a measure of the normalized averaged cross-sectional area between the k^{th} measured and reference profiles for the i^{th} armor rock weight.

In most cases the eroded volume functions computed from the measured profiles did not sum to zero at the crest of the breakwater. When the non-closure difference was positive, $EV_M^i(k,26) = \Delta_C^i(k) > 0$, it indicated that the measured accreted area, A_a, was greater than the measured eroded area, A_e. When $EV_M^i(k,26) = \Delta_C^i(k) < 0$, the opposite. A correction function, $CF^i(k,L)$, was applied by assuming: 1) a constant porosity; 2) that the eroded and accreted cross-sectional areas should be equal after each run; and 3) the S-shaped cross-sectional profiles could be approximated by a sinusoid. Corrected eroded volume functions, $EV_C^i(k,L)$, were computed from $EV_M^i(k,L)$, for the k^{th} run at station L and i^{th} armor rock weight, according to

$$EV_C^i(k,L) = EV_M^i(k,L) \begin{pmatrix} - \\ + \end{pmatrix} CF^i(k,L) \; ; \quad \begin{matrix} A_a > A_e \\ A_a < A_e \end{matrix} \tag{33}$$

where $CF^i(k,L)$ is given by

$$CF^i(k,L) = \frac{\Delta_c^i(k)}{4} \left[1 - \cos \frac{2\pi(L-l_a)}{l_e - l_a} \right] \tag{34}$$

when $l_a \leq L \leq (l_a+l_e)/2$; and

$$CF^i(k,L) = \frac{\Delta_c^i(k)}{4} \left[1 + \cos \frac{2\pi(L-l_a)}{l_e - l_a} \right] + \frac{\Delta_c^i(k)}{2} \tag{35}$$

when $(l_a+l_e)/2 \leq L \leq l_e$.

Figure 13 shows typical measured $EV_M^i(k,L)$ and corrected $EV_C^i(k,L)$ eroded volume functions. The maximum value of $EV_C^i(k,L)$ defines the dimensionless damage level, $D^i(k)$, for realization k for the i^{th} armor rock weight. $D^i(k)$ is the eroded (accreted) area normalized by $(d_n^i)^2$. Damage levels defined in this way may be more reliable than ones obtained by measuring only the eroded area since the measurement of the accreted area provides additional information about the rock distribution the armor layer. Table 4 summarizes the measured sea state parameters of the 16 sequences of realizations tested. H_{10} has been computed according to $H_{10}=5.091(m_0)^{1/2}$. Table 5 summarizes the damage data corresponding to the sea state parameters shown in Table 4.

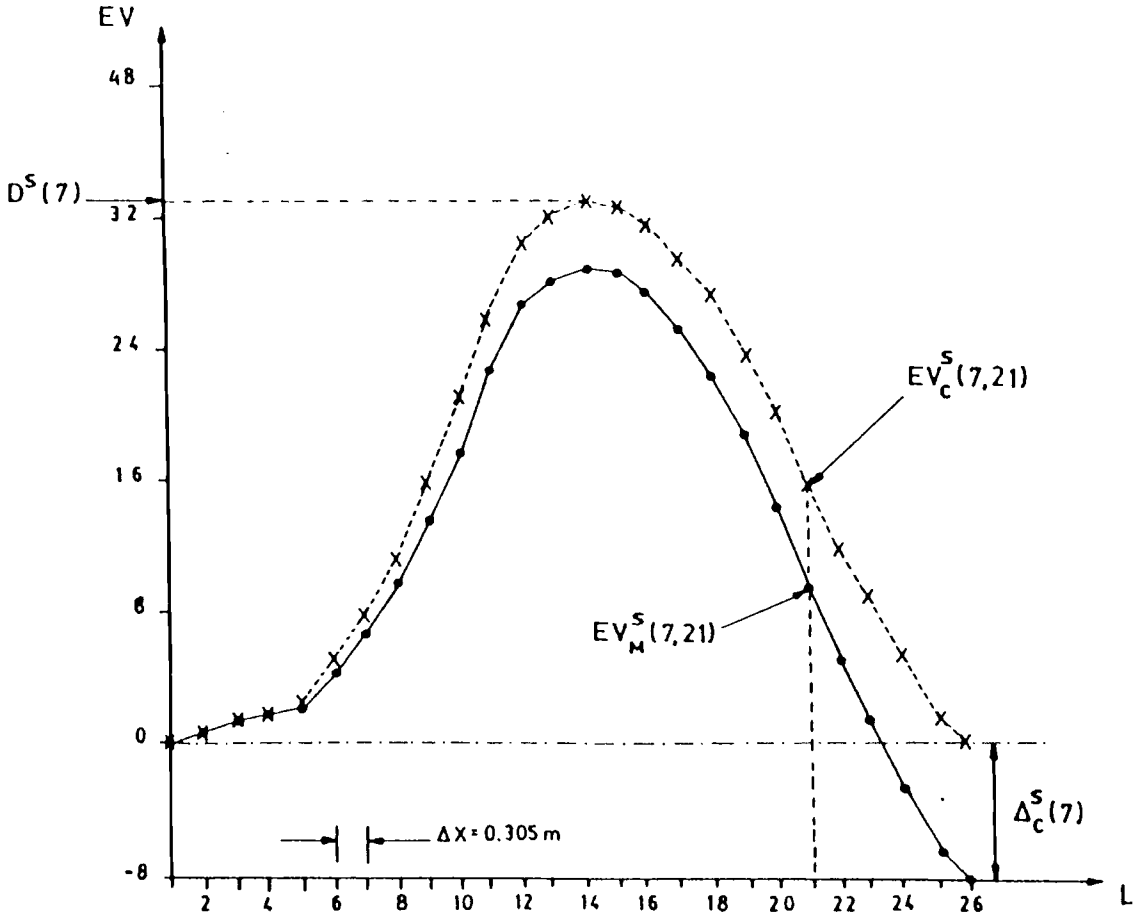

Figure 13. Measured, $EV_M^S(7,L)$, and corrected, $EV_C^S(7,L)$, eroded volume functions, non-closure value, $\Delta_c^S(7)$, and damage level $D^S(7)$ corresponding to a realization with parameters γ=10, α=1.027, ψ=0, and H_s=0.73 m.

		$\psi = 0$				$\psi = 2\pi/3$				$\psi = 4\pi/3$				$\psi = 2\pi$			
Env.(i)	Run(k)	H_{10}	α	H_{10}/H_d^L	H_{10}/H_d^S	H_{10}	α	H_{10}/H_d^L	H_{10}/H_d^S	H_{10}	α	H_{10}/H_d^L	H_{10}/H_d^S	H_{10}	α	H_{10}/H_d^L	H_{10}/H_d^S
1	1	0.568	1.710	0.948	1.044	0.578	1.936	0.965	1.063	0.566	1.694	0.945	1.040	0.580	2.910	0.968	1.066
	2	0.630	2.171	1.052	1.158	0.621	2.035	1.037	1.142	0.625	2.642	1.043	1.149	0.632	1.998	1.055	1.162
	3	0.688	2.079	1.149	1.265	0.678	1.853	1.132	1.246	0.669	1.873	1.117	1.230	0.678	1.606	1.132	1.246
	4	0.735	1.609	1.227	1.351	0.735	1.968	1.227	1.351	0.733	2.125	1.224	1.347	0.736	2.172	1.229	1.353
	5	0.788	1.630	1.316	1.449	0.806	2.132	1.346	1.482	0.801	2.008	1.337	1.472	0.797	1.801	1.331	1.465
	6	0.866	1.799	1.446	1.592	0.872	1.527	1.456	1.603	0.856	1.668	1.429	1.574	0.869	2.201	1.451	1.597
	7	0.926	1.027	1.546	1.702	0.926	1.278	1.546	1.702	0.902	1.305	1.506	1.658	0.918	1.412	1.533	1.688
2	1	0.584	1.728	0.975	1.074	0.580	2.064	0.968	1.066	0.580	1.515	0.968	1.066	0.591	1.801	0.987	1.086
	2	0.631	1.985	1.053	1.160	0.635	1.642	1.060	1.167	0.635	1.462	1.060	1.167	0.639	1.862	1.067	1.175
	3	0.685	2.069	1.144	1.259	0.697	2.166	1.164	1.281	0.687	1.313	1.147	1.263	0.689	1.167	1.150	1.267
	4	0.744	1.716	1.242	1.368	0.756	1.887	1.262	1.390	0.738	1.714	1.232	1.357	0.750	1.554	1.252	1.379
	5	0.804	1.758	1.342	1.478	0.804	1.736	1.342	1.478	0.796	1.309	1.329	1.463	0.825	1.221	1.377	1.517
	6	0.870	1.750	1.452	1.599	0.866	1.683	1.446	1.592	0.866	1.588	1.446	1.592	0.884	1.382	1.476	1.625
	7	0.918	1.582	1.533	1.688	0.918	1.429	1.533	1.688	0.918	1.506	1.533	1.688	0.918	1.506	1.533	1.688
3	1	0.584	0.515	0.975	1.074	0.580	0.613	0.968	1.066	0.585	0.516	0.977	1.075	0.584	0.558	0.975	1.074
	2	0.633	0.623	1.057	1.164	0.632	0.611	1.055	1.162	0.632	0.534	1.055	1.162	0.630	0.394	1.052	1.158
	3	0.689	0.571	1.150	1.267	0.687	0.730	1.147	1.263	0.685	0.519	1.144	1.259	0.689	0.441	1.150	1.267
	4	0.747	0.572	1.247	1.373	0.749	0.520	1.250	1.377	0.745	0.467	1.244	1.369	0.746	0.449	1.245	1.371
	5	0.809	0.645	1.351	1.487	0.811	0.646	1.354	1.491	0.815	0.581	1.361	1.498	0.814	0.448	1.359	1.496
	6	0.863	0.773	1.441	1.586	0.876	0.543	1.462	1.610	0.878	0.606	1.466	1.614	0.885	0.513	1.477	1.627
	7	0.957	0.700	1.598	1.759	0.950	0.424	1.586	1.746	0.943	0.595	1.574	1.733	0.947	0.407	1.581	1.741
4	1	0.611	0.561	1.020	1.123	0.617	0.455	1.030	1.134	0.615	0.632	1.027	1.131	0.618	0.530	1.032	1.136
	2	0.655	0.472	1.093	1.204	0.667	0.433	1.114	1.226	0.664	0.459	1.109	1.221	0.671	0.472	1.120	1.233
	3	0.717	0.549	1.197	1.318	0.722	0.565	1.205	1.327	0.723	0.564	1.207	1.329	0.726	0.582	1.212	1.335
	4	0.785	0.477	1.311	1.443	0.785	0.485	1.311	1.443	0.778	0.524	1.299	1.430	0.789	0.491	1.317	1.450
	5	0.851	0.367	1.421	1.564	0.856	0.486	1.429	1.574	0.848	0.501	1.416	1.559	0.855	0.559	1.427	1.572
	6	0.907	0.361	1.514	1.667	0.916	0.590	1.529	1.684	0.914	0.609	1.526	1.680	0.918	0.481	1.533	1.688
	7	0.959	0.365	1.601	1.763	0.974	0.522	1.626	1.790	0.967	0.426	1.614	1.778	0.969	0.392	1.618	1.781

Table 4. Measured sea state parameters of the realizations tested.

		$\psi = 0$				$\psi = 2\pi/3$				$\psi = 4\pi/3$				$\psi = 2\pi$			
Env.(i)	Run(k)	H_{10}/H_d^L	$D^L(k)$	H_{10}/H_d^S	$D^S(k)$	H_{10}/H_d^L	$D^L(k)$	H_{10}/H_d^S	$D^S(k)$	H_{10}/H_d^L	$D^L(k)$	H_{10}/H_d^S	$D^S(k)$	H_{10}/H_d^L	$D^L(k)$	H_{10}/H_d^S	$D^S(k)$
1	1	0.95	2.17	1.04	5.08	0.97	2.29	1.06	1.66	0.95	0.00	1.04	0.00	0.97	1.18	1.07	1.53
	2	1.05	2.35	1.16	2.90	1.04	2.01	1.14	3.54	1.04	0.86	1.15	1.86	1.06	1.56	1.16	1.54
	3	1.15	2.22	1.27	5.32	1.13	2.26	1.25	7.82	1.12	0.84	1.23	4.43	1.13	3.30	1.25	4.41
	4	1.23	3.47	1.35	7.52	1.23	3.87	1.35	10.27	1.22	3.50	1.35	9.50	1.23	1.36	1.36	8.70
	5	1.32	6.57	1.45	12.29	1.35	5.01	1.48	16.24	1.34	7.28	1.47	11.94	1.33	4.56	1.47	16.69
	6	1.45	6.16	1.59	20.08	1.46	6.88	1.60	19.25	1.43	9.48	1.57	16.63	1.45	7.56	1.60	22.95
	7	1.55	9.31	1.71	26.74	1.55	11.96	1.70	32.92	1.51	16.27	1.66	26.95	1.53	9.61	1.69	34.72
2	1	0.98	0.72	1.07	2.44	0.97	1.36	1.07	2.55	0.97	1.47	1.07	1.91	0.99	2.57	1.09	4.42
	2	1.05	1.58	1.16	4.64	1.06	2.02	1.17	4.20	1.06	0.56	1.17	3.71	1.07	3.04	1.18	6.97
	3	1.14	1.59	1.26	6.16	1.16	3.08	1.28	6.84	1.15	1.78	1.26	4.43	1.15	5.03	1.27	9.86
	4	1.24	3.81	1.37	12.20	1.26	4.33	1.39	7.64	1.23	1.81	1.36	6.98	1.25	6.01	1.38	12.44
	5	1.34	5.43	1.48	18.18	1.34	7.01	1.48	10.92	1.33	5.52	1.46	11.57	1.38	8.26	1.52	19.02
	6	1.45	6.82	1.60	20.11	1.45	9.19	1.59	19.65	1.45	6.07	1.59	18.60	1.48	8.83	1.63	21.95
	7	1.53	9.68	1.69	36.15	1.53	13.24	1.69	32.14	1.53	11.65	1.69	31.30	1.53	11.03	1.69	37.55
3	1	0.98	2.67	1.07	2.82	0.97	1.10	1.07	1.97	0.98	1.07	1.08	2.51	0.98	1.12	1.07	0.86
	2	1.06	2.43	1.16	1.88	1.06	0.37	1.16	2.35	1.06	0.45	1.16	3.78	1.05	0.82	1.16	1.03
	3	1.15	2.80	1.27	3.62	1.15	1.62	1.26	3.02	1.14	0.86	1.26	4.72	1.15	1.42	1.27	1.94
	4	1.25	4.15	1.37	7.34	1.25	2.02	1.38	2.86	1.24	1.99	1.37	5.92	1.25	1.66	1.38	3.06
	5	1.35	2.76	1.49	8.67	1.35	2.57	1.49	4.05	1.36	4.41	1.50	6.06	1.36	4.42	1.50	7.55
	6	1.44	6.57	1.59	13.23	1.46	5.95	1.61	5.65	1.47	5.07	1.61	8.66	1.48	6.82	1.63	12.45
	7	1.60	14.50	1.76	22.18	1.59	7.69	1.75	14.64	1.57	6.25	1.73	11.78	1.58	10.36	1.74	17.82
4	1	1.02	1.01	1.12	1.63	1.03	0.89	1.13	4.26	1.03	0.44	1.13	2.06	1.03	0.00	1.14	1.60
	2	1.09	0.00	1.20	0.56	1.11	2.44	1.23	3.05	1.11	0.59	1.22	4.16	1.12	0.33	1.23	2.33
	3	1.20	1.50	1.32	1.13	1.21	1.63	1.33	2.60	1.21	0.61	1.33	4.88	1.21	0.00	1.34	3.62
	4	1.31	3.17	1.44	3.78	1.31	2.85	1.44	6.53	1.30	1.81	1.43	5.78	1.32	2.44	1.45	6.81
	5	1.42	2.79	1.56	8.54	1.43	4.19	1.57	6.52	1.42	2.36	1.56	8.90	1.43	3.65	1.57	11.40
	6	1.51	4.72	1.67	14.51	1.53	4.66	1.68	10.64	1.53	5.42	1.68	18.17	1.53	3.68	1.69	12.70
	7	1.60	9.31	1.76	21.12	1.63	5.82	1.79	29.79	1.62	6.19	1.78	35.49	1.62	3.12	1.78	32.98

Table 5. Damage data $D^i(k)$ corresponding to the realizations tested.

7. ANALYSIS OF RESULTS

Measurements of damage at different levels of wave energy were recorded and compared to the damage data in the SPM (1984). The percent damage in the SPM (1984) is defined as the area of armor units displaced from the breakwater active zone. Assuming that the elevation of the breakwater crest is equal to the design wave height, the area of the active zone of damage for the ith armor rock weight, A_z^i, for a two-layer armor is given by

$$A_z^i = 4 d_n^i H_d^i \sqrt{1 + ctg\beta} \tag{36}$$

where, H_d^i is given by the Hudson formula [SPM (1984)] by

$$H_d^i = \Delta\, d_n^i \left(K_D ctg\beta\right)^{1/3} \tag{37}$$

According to Eq.(36) the area of the active zone of damage for the armor layers tested in the experiment (K_D=4, cotgβ=2, Δ=1.74), was approximately $A_z^i = 31\left(d_n^i\right)^2$. The damage data given in the SPM (1984) may then be reasonably approximated by

$$D = 1.6\left[\frac{H_{10}}{H_d}\right]^5 \tag{38}$$

where D = dimensionless damage.

It would also be possible to compare the experimental data with the two damage formulae proposed by Van der Meer (1988). However, the Van der Meer (1988) formulae were not used for comparisons because they depend critically on the value of the permeability parameter, κ, which is too difficult to estimate for design. According to the typical values suggested by Van der Meer (1988), the permeability of the two armor rock sections tested had estimated values of $0.1 < \kappa < 0.4$. Consequently, estimates of damage may vary as much as 50% about the average value of $\kappa=0.25$. Since the selection of the parameter κ is too subjective to use for design, the Van der Meer formulae have not been included in these comparisons.

Damage observations from realizations shifted by $\psi=0$ and $=2\pi$ were assumed to be replicates that would demonstrate the statistical variability of the experiments. Damage results obtained from the phase shifted realizations having the same length of runs and wave height variability (γ and α) demonstrated that no significant difference was observed for different realizations with the same wave groups characteristics. Damage data corresponding to the phase shifted realizations were therefore considered as replicates. A description of the analysis technique used and results are presented in Appendix B.

Figures 14 and 15 compare the experimental results for damage with Eq.(38) for similar and different values of α, γ,

and for armor rock weights W_L and W_S. A least square fit for each of the four replicates (4 values of ψ) is shown for each envelope. The sets of observations are identified by the name of the envelopes, with the characteristics shown in Table 6.

Envelope	Spectral Shape γ	Envelope Exceedance, α
E1	10	1.8
E2	1	1.6
E3	10	0.23
E4	1	0.51

Table 6. Sea states notation and corresponding wave grouping parameters.

Figure 14 compares damage data, for both armor rock weights W_L=128.5 N and W_S=99.1 N, from realizations with both high and low wave height variability for long length of runs (narrow spectrum) (a and c); and short length of runs (broad spectrum) (b and d).

Figure 14 shows that for both armor layers, the damage corresponding to envelopes E1 and E3 (γ=10; α>1 and α<1) were similar to the damage corresponding to envelopes E2 and E4 (γ=1; α>1 and α<1), respectively.

Figure 15 compares damage data, for both armor rock weights W_L=128.5 N and W_S=99.1 N, from realizations with both narrow and broad spectrum for α>1 (a and c); and α<1 (b and d).

Figure 15 shows that for both armor layers, the damage

corresponding to envelopes E1 and E2 ($\alpha>1$; $\gamma=10$ and $\gamma=1$) were consistently higher than the damage corresponding to envelopes E3 and E4 ($\alpha<1$; $\gamma=10$ and $\gamma=1$). This implies that envelopes with the same envelope exceedance coefficient α produce approximately the same damage, regardless of their spectral shape.

The experimental results shown in Figures 14 and 15 indicate that:

1) the spectral shape, which is a measure of the length of runs, has no effect on the damage of the armor layers, and
2) the wave height variability affects the level of damage.

The envelope exceedance coefficient, α, may be related to a groupiness factor, GF, defined by [Medina and Hudspeth (1987)]

$$GF = \frac{\sigma[H^2(t)]}{8m_0} \tag{39}$$

where $\sigma[\bullet]$ = standard deviation of $[\bullet]$.

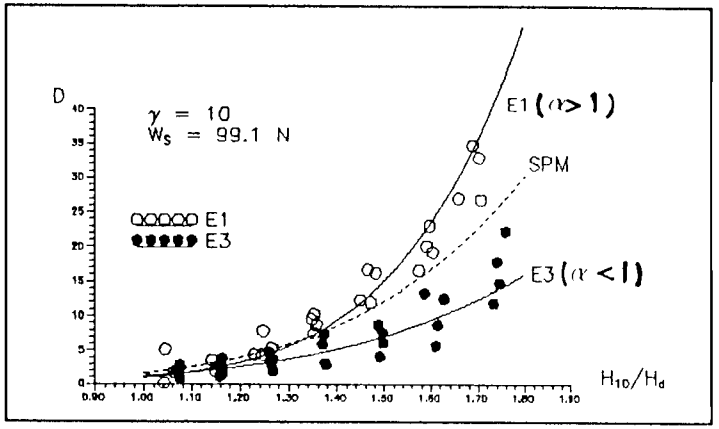

a)

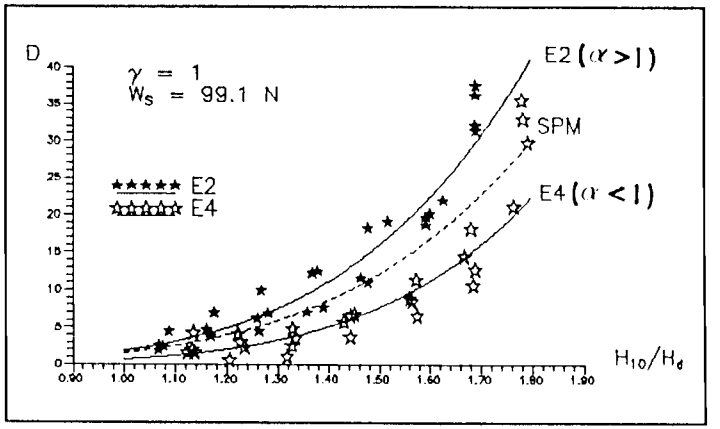

b)

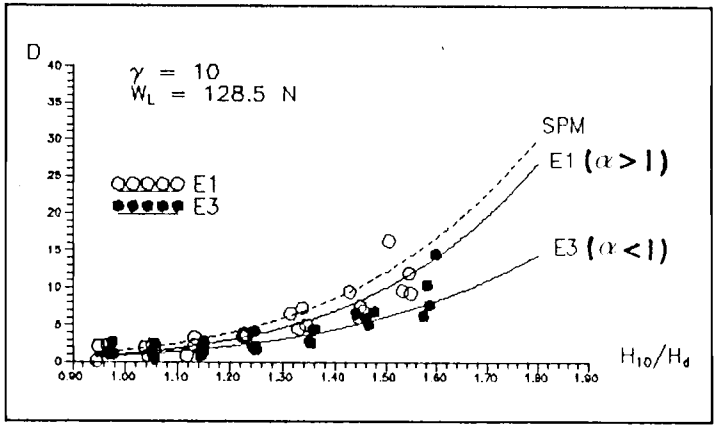

c)

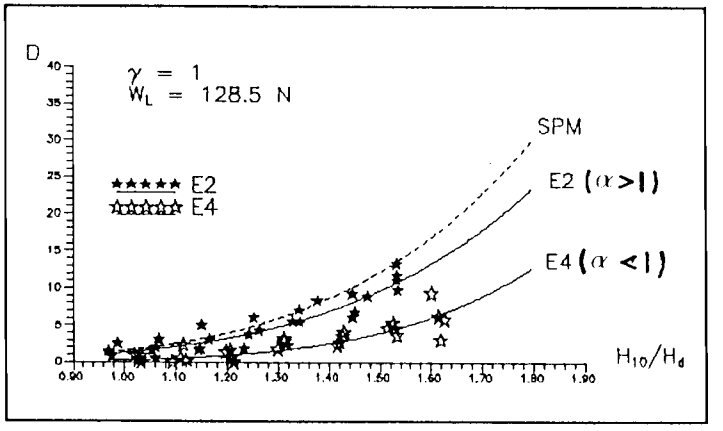

d)

Figure 14. Comparison between measured damage data and SPM(1984) damage function: a & b) small rocks; c & d) large rocks; a & c) long length of runs (γ=10); b & d) short length of runs (γ=1).

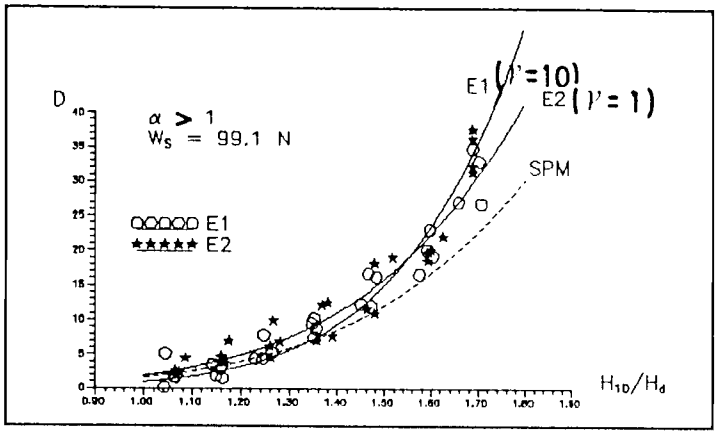

a)

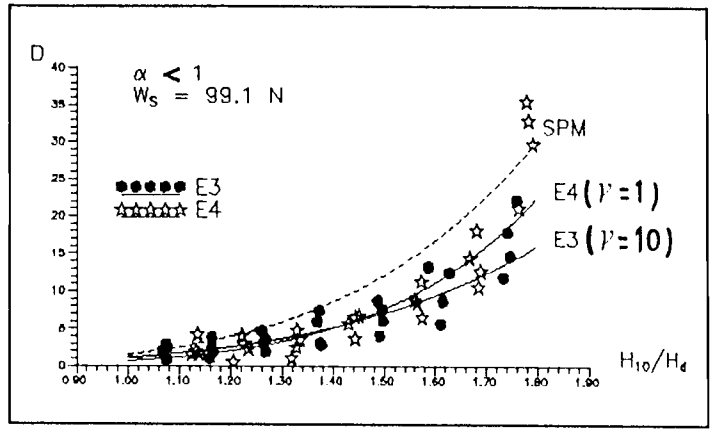

b)

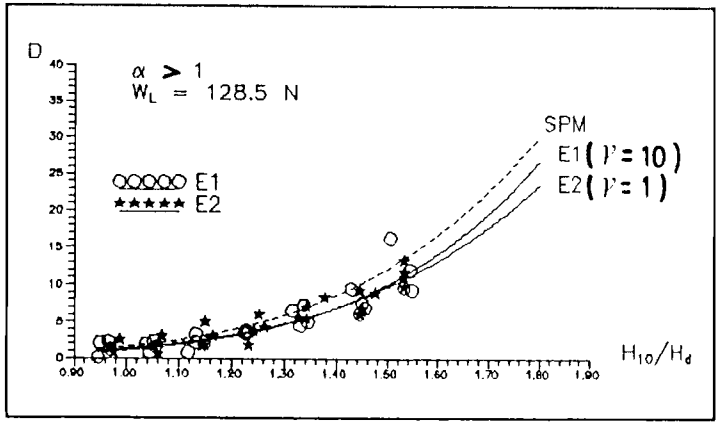

c)

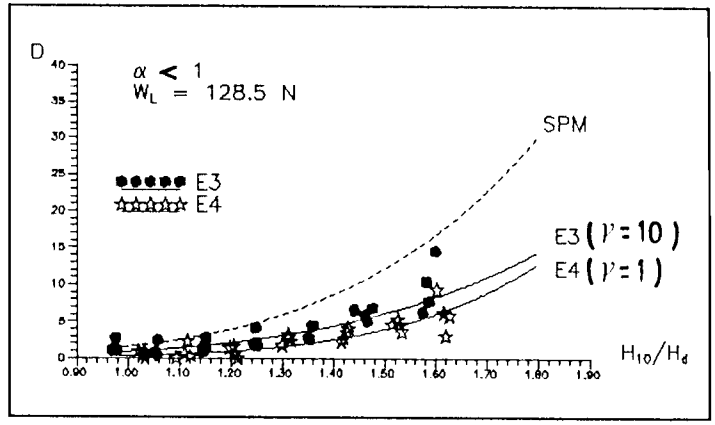

d)

Figure 15. Comparison between measured damage data and SPM(1984) damage function: a & b) small rocks; c & d) large rocks; a & c) high wave height variablity ($\alpha>1$); b & d) low wave height variablity ($\alpha<1$).

If the GF was computed by the SIWEH(t), as proposed by Funke and Mansard (1979), it would be biased and would depend on the smoothing function used. The definition for GF given by Eq.(39) was found to be highly correlated with the envelope exceedance coefficient, α, computed from analyses of 1000 DSA random simulations for the two spectral shapes used in the experiments (viz. γ=1 and γ=10). Figure 16 shows that for both values of γ, a linear relationship given by GF$\approx(9+\alpha)/10$ correlates with the simulated data.

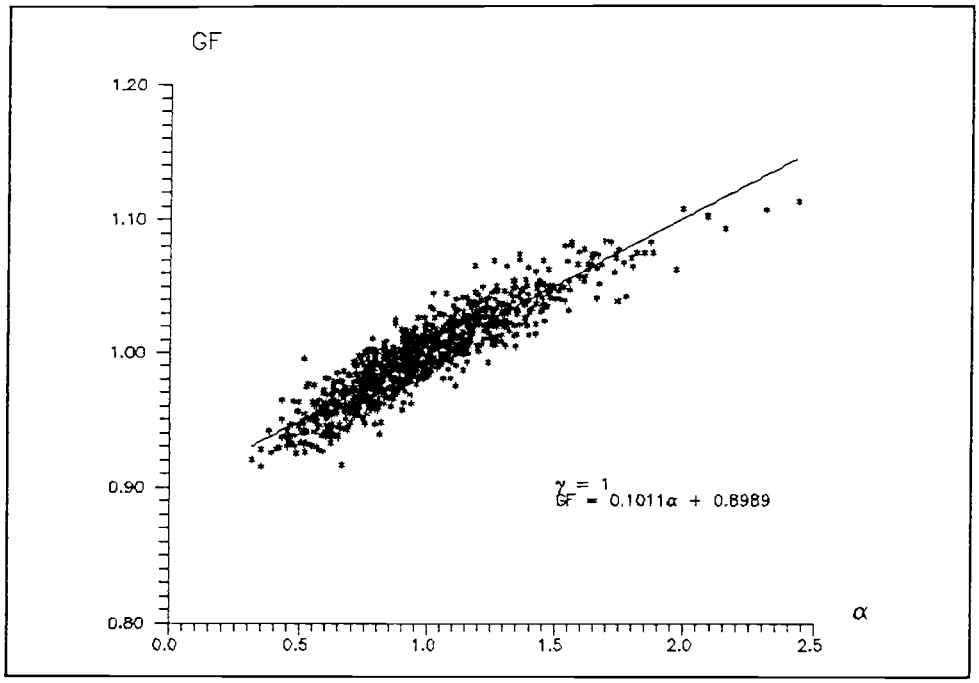

a)

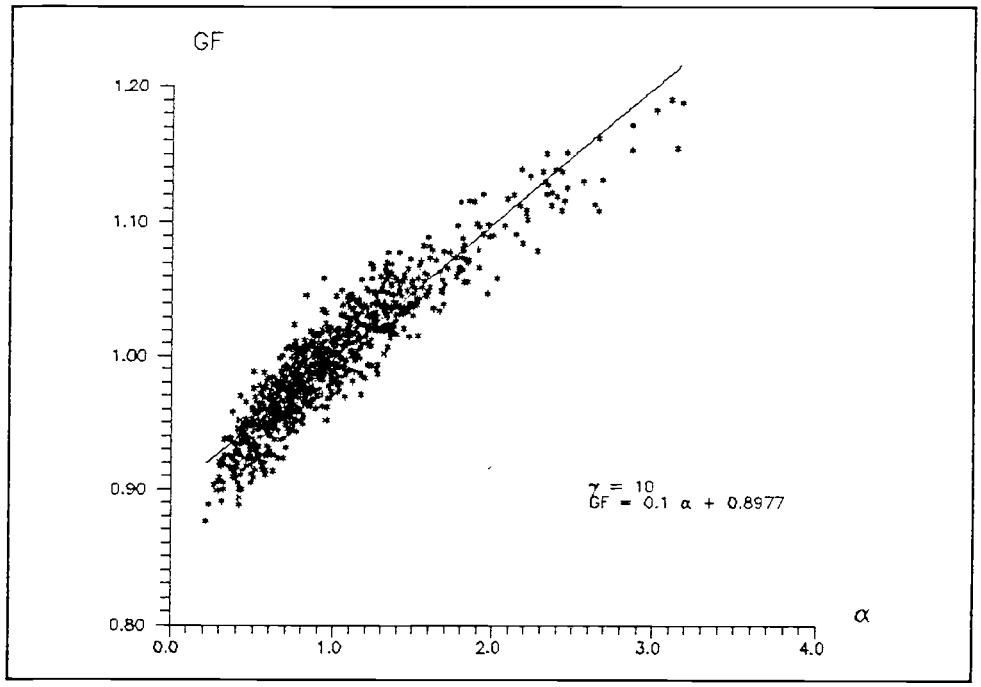

b)

Figure 16. Correlation between the groupiness factor GF and energy exceedance coefficient α for: a) short length of runs (γ=1), and b) long length of runs (γ=10).

8. SUMMARY AND CONCLUSIONS

A series of large scale experiments were conducted at the O.H. Hinsdale-Wave Research Laboratory (OHH-WRL) located on the campus of Oregon State University to evaluate the influence of wave groups on the damage of rubble mound breakwaters. The main goal of these experiments was to resolve the controversy regarding the dependency of damage on the characteristics of wave groups.

The experiments were conducted on a rough quarrystone breakwater divided in half longitudinally in order to test simultaneously two armor layers with different armor rock weights. The armor layers were tested with sequences of realizations with increasing significant wave heights. The ratio between consecutive wave heights and armor rock weights was selected so that the stability number of the small rock armor layer for realization k was equal to the stability number of the large rock armor layer for realization k+1. Under these conditions it was possible to duplicate the damage data for a given stability number.

Realizations approximately 30 minutes long were synthesized from truncated Goda-JONSWAP spectra. Wave groups were characterized by two parameters: 1) the peak enhancement factor, γ, of the Goda-JONSWAP spectrum which correlates with the length of runs; and 2) the envelope exceedance coefficient, α, which correlates with the wave height

variability. Realizations were simulated with pairs of the parameters $\{\gamma, \alpha\}$ to test the influence of both short (γ=1) and long (γ=10) length of runs and high ($\alpha > 1$) and low ($\alpha < 1$) wave height variability. The envelope exceedance coefficient α is computed from the wave height function H(t), or from the envelope A(t), of the sea surface elevation, η(t). The armor layers were tested with 4 sequences of 7 realizations with increasing wave heights. Each of the seven realizations in a sequence was shifted by a constant phase ψ=0,$2\pi/3$,$4\pi/3$, and 2π, to determine the influence of different realizations with the same wave grouping characteristics on the damage of the armor layer.

The experimental results indicated that:

1) different realizations with the same significant wave height and envelope function produced the same damage on the armor layers.
2) damage on the armor layers was not influenced by the length of runs (spectral shape).
3) the wave height variability affects the level of damage on the armor layers.

The envelope exceedance coefficient α was correlated with the groupiness factor, GF [Eq.(39)]. Random wave trains in wave channels may have exactly the same spectral shape, but produce different levels of damage to the armor layer. The groupiness parameters α or GF may be able to resolve the variability of the mean damage for a given design sea state.

BIBLIOGRAPHY

Battjes, J.A. and Vledder, V. (1984): "Verification of Kimura's Theory for Wave Group Statistics," *Proceedings,* 19th ICCE, 1984, Houston, TX, pp. 642-648.

Bendat, J.S. and Piersol, A.G. (1986): *Random Data, Analysis and Measurement Procedures*, (2nd Ed.), John Wiley, pp. 484-516.

Box, G.E.P. and Cox, D.R. (1964): "An Analysis of Transformations," *Journal of the Royal Statistical Society,* Series B, 26, pp. 211-243.

Bracewell, R.N. (1986): *The Fourier Transform and Its Applications,* (2nd Ed.), McGraw Hill, pp. 267-272.

Bruun, P. (Ed.), (1981): *Port Engineering*, (3rd Ed.), Gulf Publications, Houston, TX, pp. 209-212.

Burchart, H.F. (1979): "The Effect of Wave Grouping on On-Shore Structures," *Coastal Engineering*, No. 2, pp. 189-199.

Dugundji, J. (1958): "Envelopes and Pre-Envelopes of Real Waveforms," *IRE Transactions of Information Theory*, March 1958, pp. 53-57.

Elgar, S., Guza, R.T., and Seymour, R.J. (1984): "Groups of Waves in Shallow Water," *Journal of Geophysical Research*, Vol. 89, No. C3, pp. 3623-3634.

Elgar, S., Guza, R.T., and Seymour, R.J. (1985): "Wave Group Statistics from Numerical Simulations of a Random Sea," *Applied Ocean Research*, Vol. 7, No. 2, pp. 93-96.

Funke, E.R. and Mansard, E.P.D. (1979): "On the Synthesis of Realistic Sea States in a Laboratory Flume," *HLR Report LTR-HY 66*, National Research Council of Canada, Ottawa.

Goda, Y. (1970): "Numerical Experiments on Wave Statistics with Spectral Simulation," *Report of the Port and Harbour Research Institute*, Vol. 9, No. 3, pp. 3-57.

Goda, Y. (1983): "Analysis of Wave Grouping and Spectra of Long- Traveled Swell," *Report of the Port and Harbour Research Institute,* Vol. 22, No. 1, pp. 3-41.

Goda, Y. (1985): *Random Seas and Design of Maritime Structures*, University of Tokyo Press, p. 26.

Goda, Y. and Suzuki, Y. (1976): "Estimation of Incident and Reflected Waves in Random Waves Experiments," *Proceedings*, 15 ICCE, Honolulu, Hawaii, pp. 828-845.

Hudspeth, R.T. and Borgmann, L.E. (1979): "Efficient FFT Simulation of Digital Time Sequences," *Journal of Engineering Mechanics Division*, ASCE, Vol. 105, No. EM2, pp. 223-235.

Hudspeth, R.T. and Medina, J.R. (1988): "Wave Groups Analyses by the Hilbert Transform," *Proceedings,* 21st ICCE, 1988, Torremolinos, Spain, pp. 884-898.

Johnson, R.R., Mansard, E.P.D., and Ploeg, J. (1978): "Effects of Wave Grouping on Breakwater Stability," *Proceedings*, 16 ICCE, 1978, Hamburg, Germany, pp. 2228-2243.

Kimura, A. (1985): "The Decomposition of Incident and Reflected Random Wave Envelopes," *Coastal Engineering in Japan*, Vol. 28, pp. 59-69.

Mase, H. and Iwagaki, Y. (1986): "Wave Group Analysis from Statistical Viewpoint," *Proceedings*, OSDS '88, Corvallis, OR, pp. 145-157.

Medina, J.R. and Hudspeth, R.T. (1987): "Sea States Defined by Wave Height/Period Functions," *Proceedings*, 22nd IAHR Congress, Lausanne, Switzerland, pp. 249-259.

Medina, J.R. and Hudspeth, R.T. (1990): "A Review of the Analyses of Ocean Wave Groups," *Coastal Engineering*, No. 14, pp. 515-542.

Medina, J.R. and McDougal, W.G. (1990): "Deterministic and Probabilistic Design of Breakwater Armor Layers," (Discussion), *Journal of Waterway, Port, Coastal, and Ocean Engineering*, ASCE, Vol. 116, No. 4, pp. 508-510.

Neter, J., Wasserman, W. and Kutner, M.H. (1989): *Applied Linear Regression Models,* (2nd Ed.), Irwin, p. 149.

Rice, S.O. (1954): "Mathematical Analysis of Random Noise," *Bell System Technical Journal*, Vol. 23, 1944, and Vol. 24, 1945. (Reprinted in *Selected Papers on Noise and Stochastic Processes*, Wax. N., Ed., Dover Publications Inc. New York, NY, pp. 123-144.)

Rye, H. (1982): *Ocean Wave Groups*, Dept. Marine Technology, Norwegian Institute of Technology, Report UR-82-18.

Shore Protection Manual (1984), Coastal Engineering Research Center, Dept. of the Navy, Waterways Experiment Station, Vicksburg, Miss., pp. 7.202-7.242.

Tuah, H. and Hudspeth, R.T. (1982): "Comparisons of Numerical Random Sea Simulations," *Journal of the Waterway, Port, Coastal and Ocean Division*, ASCE, Vol. 108, No. WW4, pp. 569-584.

Van der Meer, J.W. (1988): "Deterministic and Probabilistic Design of Breakwater Armor Layers," *Journal of Waterway, Port, Coastal, and Ocean Engineering*, ASCE, Vol. 114, No. 1, pp. 66-80.

APPENDICES

APPENDIX A.- STATIONARITY ANALYSIS

The results of the wave data analyses may be significantly influenced by the stationarity of the data. Therefore, a stationarity test was performed on the wave data collected.

Assuming that the nonstationarity characteristics of a process may be revealed by time trends in the variance of the data the stationarity of random time series can be tested as follows [Bendat and Piersol (1986)]: a) divide the time series into intervals of equal time length where the data in each interval is considered to be independent; b) compute the variance for each interval and align these sample values in a time sequence; c) test the sequence of variances for the presence of underlying trends or variations other than those due to expected sampling variations.

The reverse arrangements test [Bendat and Piersol (1986)] was the technique selected to detect monotonic time trends in the measured wave data. It is hypothesized that the sequence of sample variances represents independent sample measurements of a stationary random variable with variance, σ^2. If this hypothesis is true, the variations in the sequence of sample values will be random and display no trends. The number of reverse arrangements, RA, will be as expected for a sequence of independent random observations of the stationary random variable. If the number of reverse arrangements is significantly different from this number, the

hypothesis of stationarity would be rejected. Otherwise, the hypothesis would be accepted.

Following the procedure outlined by Bendat and Piersol (1986) 6 wave time series were selected at random and tested for stationarity. Each of the N = 32768 points long time series were divided into K = 32 subrecords of N = 1024 points each. The significant wave height of each subrecord was computed and the number of reverse arrangements, RA, was calculated.

From the set of sampled variances σ^2_1, σ^2_2, ...,σ^2_N, define

$$h_{ij} = \begin{cases} 1 \ , \ if \ \sigma_i^2 > \sigma_j^2 \\ 0 \ \ otherwise \end{cases} \tag{40}$$

The number of reverse arrangements is defined as

$$RA = \sum_{i=1}^{N-1} RA_i \tag{41}$$

where

$$RA_i = \sum_{j=i+1}^{N} h_{ij} \tag{42}$$

Table 7 shows the number of reverse arrangements for the time series recorded at wave gage locations 1, 2, and 3 for 2 realizations.

	H_S (m)			H_S (m)		
Subrecord	1	2	3	1	2	3
1	0.603	0.571	0.582	0.596	0.564	0.581
2	0.716	0.653	0.658	0.728	0.683	0.706
3	0.669	0.665	0.653	0.648	0.708	0.699
4	0.593	0.624	0.658	0.560	0.581	0.609
5	0.807	0.710	0.699	0.796	0.705	0.671
6	0.933	0.910	0.868	0.954	0.924	0.903
7	0.794	0.772	0.738	0.807	0.801	0.760
8	1.369	1.231	1.132	1.272	1.173	1.048
9	0.884	0.911	0.915	0.870	0.892	0.860
10	0.865	0.869	0.857	0.822	0.803	0.789
11	0.883	0.886	0.891	0.818	0.816	0.795
12	0.712	0.691	0.684	0.675	0.659	0.652
13	0.710	0.679	0.659	0.690	0.626	0.614
14	0.666	0.672	0.666	0.614	0.639	0.645
15	0.937	0.907	0.897	0.892	0.910	0.863
16	1.005	0.946	0.918	0.987	0.960	0.925
17	0.999	0.987	0.955	0.905	0.868	0.824
18	0.701	0.725	0.714	0.776	0.758	0.742
19	0.861	0.833	0.800	0.846	0.822	0.778
20	0.785	0.786	0.757	0.758	0.774	0.764
21	0.815	0.862	0.840	0.750	0.801	0.786
22	0.583	0.582	0.564	0.558	0.547	0.553
23	0.587	0.578	0.564	0.609	0.589	0.584
24	0.762	0.684	0.721	0.731	0.674	0.694
25	0.791	0.765	0.718	0.752	0.754	0.701
26	0.812	0.768	0.751	0.822	0.769	0.699
27	0.901	0.874	0.812	0.872	0.870	0.858
28	0.809	0.826	0.835	0.758	0.784	0.760
29	0.866	0.831	0.824	0.810	0.767	0.759
30	0.654	0.636	0.632	0.651	0.645	0.632
31	0.570	0.567	0.552	0.575	0.577	0.549
32	0.694	0.663	0.673	0.715	0.682	0.661

RA	267	261	253	265	268	278

Table 7. Number of reversed arrangements, RA, for two realizations at wage gage locations 1,2, and 3.

The region of acceptance of the hypothesis is given by

$$RA_{(K,1-\frac{\nu}{2})} < RA < RA_{(K,\frac{\nu}{2})} \tag{43}$$

where K = number of subrecords, and ν = level of significance. From the reverse arrangements distribution table, and for K = 32 and ν = 0.05 the limiting values in Eq.(34) are

$$RA_{(32,0.975)} = 191 \quad ; \quad RA_{(32,0.025)} = 312 \tag{44}$$

Therefore, since the number of reverse arrangements computed for each time series agrees with

$$191 < RA < 312 \tag{45}$$

the hypothesis of stationary can be accepted with a 5% level of significance.

APPENDIX B.- STATISTICAL ANALYSIS OF DAMAGE

In order to test if different realizations with the same wave groups characteristics produce the same damage on the structure the following statistical analysis was performed. First, the repeatability of the experiments was tested. Damage data corresponding to realizations, with the same wave groups characteristics $\{\gamma, \alpha\}$ phase shifted by $\psi=0$ and $\psi=2\pi$ were compared. Second, it was tested if the 4 phase-shifted realizations ($\psi=0$, $2\pi/3$, $4\pi/3$, and 2π) with equal pairs $\{\gamma, \alpha\}$ produce the same damage on the structure. Multiple linear regression has been used to analyze the damage data.

In general, the damage data showed a power relation with an increasing error variance. In order to apply the multiple linear regression analysis a transformation on the damage level variable D, of the form

$$D' = D^{\chi} \tag{37}$$

was needed to stabilize the variance of the error and to obtain a linear relationship [Neter et al. (1989)]. Box-Cox transformations [Box and Cox (1964)] were applied to choose, in each case, a transformation from the families of the power transformations on D. The criterion for selecting the parameter χ with this approach consists in finding the value of χ that minimizes the residual sum of squares (RSS) for a linear regression based on that transformation.

The proposed multiple linear regression analysis consists of fitting regression lines to K groups of data with three different models; $model_1$: K non-parallel lines, $model_2$: K parallel lines, and $model_3$: one line. For each model the residual sum of squares (RSS) is computed. An F-Test between models is then performed to decide if one model is as good as the other. $Model_{(i-1)}$ has been considered as the alternative model. The F-Test for models i=2 and 3 is given by

$$F_i = \frac{(RSS_i - RSS_{i-1}) \;/\; (DF_i - DF_{i-1})}{RSS_{i-1} \;/\; DF_{i-1}} \qquad (47)$$

where RSS = residual sum of squares, and DF = degrees of freedom of the model. If the hypothesis provides as good a model as does the alternative, then the F statistic will be small when compared to the percentage points of the $F(DF_i-DF_{i-1}, DF_{i-1}, \nu)$ distribution, where ν = level of significance. If the hypothesized models (2 and 3) are not rejected then it can be concluded that differences between the damage data collected are only due to random variability.

The models mentioned are conveniently formulated by the following sets of equations:

a) Two groups of data (replicates)

$Model_1$: 2 non-parallel lines.

$$D_j = \epsilon_0 + \epsilon_1 H_j + \epsilon_2 Z_j + \epsilon_3 Z_j H_j \;; \quad \text{for } j=1 \text{ to } 14 \qquad (48)$$

where D_j = damage level, ϵ_i = regression line parameters, H_j = H_{10}/H_d for the corresponding damage, and Z_j identifies groups. In this case, Z_j = 1 indicates the first replicate; 0 otherwise. Since damage data corresponding to the second replicate is uniquely identified by Z_j = 0 both groups can be identified by this single variable.

Model$_2$: 2 parallel lines.

The same reasoning as before applies, but the model is now constrained to compute a common slope for both groups,

$$D_j = \epsilon_0 + \epsilon_1 H_j + \epsilon_2 Z_j \; ; \quad \text{for } j=1 \text{ to } 14 \tag{49}$$

Model$_3$: one line.

The simple regression equation is used,

$$D_j = \epsilon_0 + \epsilon_1 H_j \; ; \quad \text{for } j=1 \text{ to } 14 \tag{50}$$

b) Three groups of data (phase shifted realizations)

Model$_1$: three non-parallel lines.

$$D_j = \epsilon_0 + \epsilon_1 H_j + \epsilon_2 Z_{1j} + \epsilon_3 Z_{2j} + \epsilon_4 Z_{1j} H_j + \epsilon_5 Z_{2j} H_j \; ; \quad \text{for } j=1 \text{ to } 28 \tag{51}$$

Model$_2$: three parallel lines

$$D_j = \epsilon_0 + \epsilon_1 H_j + \epsilon_2 Z_{1j} + \epsilon_3 Z_{2j} \; ; \quad \text{for } j=1 \text{ to } 28 \tag{52}$$

Model$_3$: one line

$$D_j = \epsilon_0 + \epsilon_1 H_j \; ; \quad \text{for } j=1 \text{ to } 28 \tag{53}$$

Again, additional variables have been defined in order to identify damage data corresponding to the phase-shifted realizations,

Z_{1j} = 1 if phase shift is ψ = 0 and 2π; 0 otherwise

Z_{2j} = 1 if phase shift is $\psi = 2\pi/3$; 0 otherwise

All models explained above can conveniently be written in matrix notation as,

$$\vec{D} = \vec{H} . \vec{\epsilon} \tag{54}$$

where $\vec{D}$ = the damage vector, $\vec{H}$ = matrix that gives the observed values of the predictors appended to a column of 1's as the leftmost column, and $\vec{\epsilon}$ is the parameter vector. The i^{th} row of $\vec{H}$ and $\vec{D}$ corresponds to values of the i^{th} case of the data while the columns correspond to the different predictors. The cases were ordered by increasing values of H_j.

Table 8 shows the analysis of the replicates based on the F-Test.

		W = 128.5 N				W = 99.1 N			
		E_1	E_2	E_3	E_4	E_1	E_2	E_3	E_4
Model 1	RSS_1	0.076	1.170	0.079	0.920	0.555	0.025	0.120	0.115
Model 2	RSS_2	0.094	1.330	0.094	0.920	1.070	0.035	0.140	0.117
	F_2	2.37	1.37	1.90	0.00	9.28	4.00	1.68	0.20
	F [1,10,0.025]	6.94	6.94	6.94	6.94	***	6.94	6.94	6.94
Model 3	RSS_3	0.097	5.950	0.140	1.350	***	0.043	0.330	0.158
	F_3	0.35	38.00	5.38	5.14	***	2.51	14.92	3.89
	F [1,11,0.025]	6.72	***	6.72	6.72	***	6.72	***	6.72

*** = Fails

Table 8. F-Test results for damage of replicate realizations.

It was concluded from the results shown in Table 8 that the damage produced by two identical realizations was the same. The influence on damage of different realizations with the equal $\{\gamma, \alpha\}$ was analyzed next. Damage data was grouped according to the corresponding phase shift: group 1: $\psi=0$ and 2π, group 2: $\psi=2\pi/3$, and group 3: $\psi=4\pi/3$. Table 9 shows the analysis of the phase shifted realizations based on the F-Test.

It was concluded from the results shown in Table 9 that the damage produced by the phase shifted realizations was the same. Therefore it can be hypothesized that different realizations which have the same wave groups characteristics $\{\gamma, \alpha\}$ will produce the same damage on the structure.

		W = 128.5 N				W = 99.1 N			
		E_1	E_2	E_3	E_4	E_1	E_2	E_3	E_4
Model 1	RSS_1	1.130	2.025	0.639	2.638	3.320	0.010	0.150	0.304
Model 2	RSS_2	3.230	2.160	0.639	2.900	3.490	0.011	0.240	0.350
	F_2	20.40	0.73	0.00	1.09	0.58	1.22	6.60	1.66
	F [2,22,0.025]	***	4.38	4.38	4.38	4.38	4.38	***	4.38
Model 3	RSS_3	***	2.750	0.866	3.390	4.140	0.022	***	0.413
	F_3	***	3.28	4.26	2.02	2.23	11.78	***	2.16
	F [2,24,0.025]	***	4.32	4.32	4.32	4.32	***	***	4.32

*** = Fails

Table 9. F-Test results for damage of phase shifted realizations.